

ANALYTICAL INVESTIGATION OF
STABILITY OF SQUEEZE-FILM
JOURNAL BEARINGS

Thesis for the Degree of Ph. D.
MICHIGAN STATE UNIVERSITY
John Edward Nolan
1966

LIBRARY
Michigan State
University

This is to certify that the

thesis entitled

ANALYTICAL INVESTIGATION OF STABILITY
OF SQUEEZE-FILM JOURNAL BEARINGS

presented by

John Edward Nolan

has been accepted towards fulfillment
of the requirements for

Ph.D. degree in M. E.

RT Hinkle

Major professor

Date Nov-23, 1966

ABSTRACT

ANALYTICAL INVESTIGATION OF STABILITY OF SQUEEZE-FILM JOURNAL BEARINGS

by John Edward Nolan

Because of increasing applications for gas bearings, the operating characteristics of such bearings, in particular, stability characteristics, are of interest. While many investigators have considered hydrodynamic and externally-pressurized gas bearings in this regard, very little has been done with squeeze-film type gas bearings.

This paper describes the investigation of stability characteristics of squeeze-film type gas journal bearings by solving the differential equations which describe bearing behavior--Reynolds' equation and the dynamic equations for the journal. Although some approximate results were obtained from small-parameter considerations leading to forms of the Mathieu equation, the greatest accuracy was given by digital-computer solutions based on finite-difference methods. A technique was devised which enables the computer to automatically locate and follow the boundaries of stability maps, even

around extremely sharp turns. The associated logic is described in detail and is adaptable to the determination of boundaries in other similar applications.

After a thorough analysis of an infinitely-long journal bearing constrained to motion in only one translational coordinate, the work was extended to include (a) bearings of finite length and (b) bearings allowed to tilt as well as translate in one plane. Of all cases considered, it was found that the stability regions for the infinite journal were the smallest. Thus, it was concluded that a bearing design based on the characteristics for an infinite journal would be conservative.

ANALYTICAL INVESTIGATION OF STABILITY
OF SQUEEZE-FILM JOURNAL BEARINGS

By

John Edward Nolan

A THESIS

Submitted to
Michigan State University
in partial fulfillment of the requirements
for the degree of

DOCTOR OF PHILOSOPHY

Department of Mechanical Engineering

1966

842322
4/7/61

ACKNOWLEDGMENTS

During the research for and preparation of this thesis, the author has become indebted to many people for their help, understanding, and encouragement. The work of his guidance committee; Professors Rolland T. Hinkle, George H. Martin, James V. Beck, George E. Mase, and Edward A. Nordhaus; throughout the doctoral program, is much appreciated. Special thanks are due to Professor Hinkle for serving as chairman of this committee, and to Professor Beck for his excellent guidance of the research for the thesis.

The author is also grateful to Lear-Siegler, Incorporated for bringing the gas-bearing problem to Michigan State University and for their financial support of the research during the summer of 1965.

Finally, the author would like to thank his family for their understanding and encouragement throughout his graduate program.

TABLE OF CONTENTS

	Page
ACKNOWLEDGMENTS	ii
LIST OF FIGURES	v
LIST OF TABLES	vii
LIST OF APPENDICES	viii
LIST OF SYMBOLS	ix
INTRODUCTION	1
STABILITY OF THE INFINITE JOURNAL BEARING IN ONE DEGREE OF FREEDOM	7
The Reynolds Equation	9
The Equation of Motion	12
Determining Stability	13
Simplified Reynolds Equation for Large σ	15
A "Mass-Content" Rule	15
Stability of the Infinite Journal	17
Compatible Values of Parameters	18
Solution of the Equation of Motion	20
The Results of Beck and Strodman	24
The "Automatic" Program	27
Finding the "Hole" Automatically	32
Comparison of Some Y Responses	36
Speeding-up the Process	43
Other Values of W'	52
STABILITY OF THE FINITE JOURNAL BEARING IN ONE DEGREE OF FREEDOM	58
Mass-Content Rule for Finite Bearings	58
Equation of Motion for Finite Bearings	64
Searching in Other Coordinates	65
Plots of ϵ_2 versus B^{-1} Independent of $\frac{L}{R}$	69
Constructing Stability Plots For Finite Journals	71
Comparison of Finite and Infinite Bearings	77

STABILITY OF THE FINITE JOURNAL BEARING IN MORE-THAN-ONE DEGREE OF FREEDOM	78
Some Analytical Considerations	82
Some Computer Results for Two Degrees of Freedom	91
Motion in the Angular Coordinate Only	94
Back to Motion in Both Coordinates	97
CONCLUSIONS	100
LIST OF REFERENCES	102

LIST OF FIGURES

Figure	Page
1. End view of the shaft indicating nomenclature	10
2. End view of the shaft showing the action of a general pressure force	10
3. The load-support curves for an infinite journal given by Ref. [1]	21
4. The stability curves for an infinite journal given by Ref. [1]	25
5. Graphical presentation of the automatic seeking method	28
6. The first stability plot from an automatic program; for $W'=0.1$	33
7. Stability plot for $W'=0.1$ showing detailed construction of the hole . .	35
8. Typical response plots for points in the vicinity of point J of Fig. 7 . .	38
9. Typical response plots for points from point G to point H of Fig. 7	40 41 42
10. Typical response plots for points in the vicinity of point L of Fig. 7 . .	44
11. Stability plot for $W'=0.1$, $CRD=0.5$, superimposed over the plot of Fig. 7 .	48
12. Stability plot for $W'=0.1$, $CRD=0.25$, superimposed over the plot of Fig. 7 .	49
13. Stability plot for $W'=0.1$, $CRD=0.1$, superimposed over the plot of Fig. 7 .	51
14. Stability plots for $W'=0.6, 0.5, 0.4$, and 0.3 ; based on $CRD=0.1$; superimposed over the corresponding curves from Fig. 4	53

Figure	Page
15. Stability plots for $W'=0.2$ and 0.15 , based on $CRD=0.1$, superimposed over the corresponding curves from Fig. 4	54
16. Stability plots for $W'=0.05$, 0.025 , 0.01 , and 0.001 ; based on $CRD=0.1$; superimposed over the curves from Fig. 4 for $W'=0.05$, 0.025 , and 0.0	55
17. Load-support curves for bearings with a length-to-radius ratio of unity	62
18. Load-support curves for bearings with a length-to-radius ratio of 2.0	63
19. Stability plots of ϵ_2 versus B^{-1} for $\epsilon_1=0.8$, 0.5 , and 0.3 ; constructed from the data of Figs. 13-16	68
20. Stability plots of ϵ_2 versus B^{-1} for $\epsilon_1=0.8$, 0.5 , and 0.3 ; $\frac{L}{R}=2.0$; superimposed over the corresponding curves for infinite bearings	70
21. Stability plots of ϵ_2 versus B^{-1} for various constant ϵ_1 , based on the program for infinite journals	73
22. Partial stability plots of ϵ_1 versus B^{-1} for $\frac{L}{R}=1.0$, superimposed over the corresponding plots for an infinite journal ($W'=0.15$ and 0.2)	75
23. Partial stability plots of ϵ_1 versus B^{-1} for $\frac{L}{R}=1.0$, superimposed over the corresponding plots for an infinite journal ($W'=0.3$, 0.4 , and 0.5)	76
24. Configuration of the two-degree-of-freedom system	79
25. Stable and unstable regions for the Mathieu equation	88
A-1 Flow chart for the automatic curve-following logic	105

LIST OF TABLES

Table	Page
1. Comparison of computed values of B^{-1} with those predicted by Eq. (65)	95

LIST OF APPENDICES

Appendix	Page
A (A discussion of the computer logic for the automatic curve-following technique)	104

LIST OF SYMBOLS

(The page of first mention for each symbol
is indicated in parentheses.)

- ARG** --a FORTRAN name for the angle which defines the direction of advance in the automatic programs (p. 29)
- B** --a dimensionless group defined as $B = \frac{mh_0\omega^2}{g_0 p_a RL}$ (p. 13)
- CRD** --defined on p. 46
- CRD2** --defined on p. 92
- DELARG** --the increment used to change **ARG** as required (p. 29)
- DIST** --the distance between consecutive points tested in the automatic programs (p. 29; further description on p. 31)
- g_0** --conversion factor which depends on the system of units used (p. 13)
- h** --the film thickness at a given z, θ, τ (p. 11)
- H** --normalized h (p. 11)
- h_0** --the nominal clearance between journal and bearing (p. 8)
- h_1** --amplitude of the squeeze motion (p. 8)
- J** --moment of inertia of the journal about a line through its center of gravity perpendicular to its axis (p. 81)
- L** --length of the journal (p. 8)
- m** --mass of the journal (p. 8)
- p** --the pressure in the film at a given z, θ, τ (p. 11)
- P** --normalized p (p. 11)
- p_a** --ambient pressure (p. 11)

R --radius of the journal (p. 8)
 t --normalized time (p. 11)
 T --defined as $T=\psi^2$ (p. 59)
 W_1 --load per unit length of journal due to shaft weight and applied forces (p. 13)
 W' --a dimensionless group defined as $W'=\frac{W_1}{2p_a R}$ (p. 13)
 y --the coordinate which specifies the location of the center of gravity of the journal (p. 9)
 Y --normalized y (p. 14)
 Y_0 --initial value of Y (p. 22)
 z --coordinate of position along the journal, measured from the left end (p. 9)
 Z --normalized z (p. 11)
 ΔY --the variation in Y used in the small-parameter analysis (p. 87)
 ϵ_1 --normalized squeeze amplitude; excursion (p. 14)
 ϵ_2 --the normalized average equilibrium position of the journal in the Y coordinate (p. 16)
 θ --angular position coordinate around the journal (p. 9)
 λ --defined by Eq. (21), (p. 18)
 μ --viscosity of the gas film (p. 11)
 ρ --density of the gas film (p. 11)
 σ --squeeze number (p. 12)
 τ --real time (p. 11)
 ϕ --the angular coordinate which specifies the tilt of the journal (p. 80)
 ϕ' --defined as $\phi'=\frac{R}{h_0}\phi$ (p. 81)
 Ψ --defined as $\Psi=PH$ (p. 16)
 ω --squeeze frequency (p. 11)

INTRODUCTION

In the present space-age technology, there is an increasing demand for bearings which can operate over a wide speed range, with low friction, and under extreme conditions of environment. This demand is being met in certain applications with the use of gas bearings, i.e., bearings which use a gas (e.g., air) as their lubricant. It is desired that the load applied to these bearings be supported entirely by the film of gas which exists between the bearing surfaces. In order for such a film to support a load, the pressure forces in the film must be such that their resultant produces a net lift. There are basically three different methods of effecting suitable pressure distributions, and gas bearings are classified according to which of these means they are designed to use. The three general classifications of gas bearings are: (1) self-acting, or hydrodynamic, bearings, (2) externally-pressurized bearings, and (3) squeeze-film type gas bearings. Each of these types will be described briefly below for the particular case of journal bearings, although it should be clear that gas bearings can be used in other configurations (e.g., thrust bearings) as well.

In hydrodynamic bearings, the relative tangential motion of the bearing surfaces results in gas being carried around and wedged into the space of minimum clearance, thus effecting a lift. Since the operation of these bearings is dependent on the relative motion of the bearing surfaces, self-acting bearings are limited to applications where such relative motion is always present; e.g., in the case of journal bearings, the journal must always be rotating.

When there is insufficient relative surface motion to develop a self-acting film, or when wide speed fluctuations are expected, either an externally-pressurized bearing or a squeeze-film bearing must be used. A typical application for low-speed, low-friction bearings is in gimbal bearings for gyroscopes.

The lift in an externally-pressurized bearing is produced by gas being forced under pressure into the space between the bearing surfaces. The gas can be fed into the bearing through orifices, capillary restriction holes, or grooves.

The net supporting force in squeeze-film bearings is created by oscillating one of the bearing surfaces rapidly in-and-out normal to the film. Since the pressure increase during the approach is of greater magnitude than the pressure decrease during the pull-away part of the cycle, a net positive lift results. In the

case of a journal bearing, an overall net force on the journal can be produced only if the journal is not concentric with the bearing. If the journal is off center, the tendency of the squeeze-film pressure forces is to return it to the center. Either externally-pressurized or squeeze-film journal bearings can support a load even if the journal is not rotating. If it is rotating, the self-acting lift effects resulting from this rotation should generally be expected to combine with the externally-pressured or squeeze-film effects.

Experience with self-acting and externally-pressurized gas bearings has shown that, while the pressure forces developed may be sufficient to support the required load, certain operating conditions do not allow the journal to seek a stable equilibrium position and remain there, but instead cause it to move about inside the bearing, possibly until the journal and bearing come into contact. These undesirable bearing phenomena are commonly called forms of instability.

While stability characteristics of self-acting and externally-pressurized bearings have been studied by many investigators, both experimentally and analytically, very little has been published about squeeze-film bearings. An initial investigation by Beck and Strodman [1]¹

¹Numbers in brackets designate references.

showed that these bearings also exhibit stable and unstable regions of operation. It is the purpose of the present work to make a more-complete determination of these regions and to extend the analysis to bearings of finite length which are free to move in more than one degree of freedom.

In the analytical investigation of gas bearings of any of the three basic types, the partial differential equation describing the fluid flow and pressure distribution in the bearing (Reynolds' equation) must be satisfied. If the Reynolds equation is solved by itself, with the journal in some specific configuration, only pressure distribution and load support information can be obtained. If stability characteristics are to be determined, appropriate equations of motion for the journal must be solved concurrently with the Reynolds equation. The equations of motion are invariably based on Newton's second law and are relatively easy to solve. Reynolds' equation, on the other hand, is a rather cumbersome partial differential equation; the various methods which have been used to satisfy it will now be reviewed.

Numerous perturbation techniques have been applied to the Reynolds equation. In these methods, a solution is assumed as a power series in terms of a parameter appropriate to the nature of the problem. Gross and Zachmanoglou [2] discuss several of the perturbation param-

eters which have been considered. Ausman was the first to use the product PH (where P and H are normalized pressure and clearance respectively) as the basis of a perturbation series, and most subsequent perturbation approaches have used his "Linearized PH Method" [3].

Galerkin's method has been used by some investigators [4,5]. In this method, the Reynolds equation is reduced to a system of first-order ordinary differential equations which are then solved together with the equations of motion.

Castelli and Elrod [6] used a finite-difference approach, solving both the Reynolds equation and the dynamic equations for the journal on a digital computer. While this method is very expensive, it also results in greater accuracy than the others, as pointed out by Ausman [7].

For further reference concerning these methods, the papers of Katto and Soda [8] and Pan and Sternlicht [9] are recommended. The first of these compares theoretical methods of solving the Reynolds equation, and the second compares both theoretical and experimental methods of determining stability of self-acting plain cylindrical journal bearings.

The only papers concerning squeeze-film bearings known to be presently published are those of Salbu [10]; Pan, Malanoski, Broussard, and Burch [11]; and Beck and

Strodtman [1]. Salbu's paper compares experimental results with finite-difference solutions of the squeeze-film equations for a pair of parallel coaxial disks. Reference [11] compares various theoretical and experimental results for squeeze-film cylindrical journal bearings. Neither of these two papers consider stability. Reference [1] does outline approximate stability maps for infinite squeeze-film journal bearings, and these results will be extended in the present investigation.

The methods mentioned above for solving the Reynolds equation were all used for either self-acting or externally-pressurized journal bearings. In the present investigation, it will be seen that, for the squeeze-film configurations considered, the Reynolds equation will reduce to a relatively simple form. The dynamic equations are then solved by finite-difference methods, subject to the restrictions imposed by the simplified Reynolds equation and by a mass-content rule. Of the various methods discussed above, the present method is most like that of [6].

The computer used throughout this work was the Control Data Corporation 3600 at Michigan State University. The plotter used in conjunction with this computer was the CDC 165.

STABILITY OF THE INFINITE JOURNAL BEARING IN ONE DEGREE OF FREEDOM

It is desired to establish stability characteristics of squeeze-film type gas journal bearings. The method of determining these characteristics is basically a computer-solution of the differential equations governing bearing behavior. These equations are of two types: (1) the equation relating properties within the gas film (Reynolds' equation) and (2) the equation (or equations) of motion of the journal in response to forces which are applied to it by the pressure of the gas film, by any external loads which may be applied, and by the weight of the journal itself. These latter equations are derived from Newton's second law of motion.

In order to completely locate a rigid body in space, six independent coordinates are required. Thus, in order to provide for the most general motion of the journal, equations of motion in each of six coordinates should be used. If it is desired to eliminate consideration of motion in one or more of these coordinates, appropriate constraints should be assumed. Because it is not likely that a journal would move an appreciable distance along its axis, motion in this coordinate will be neglected.

Because squeeze-film effects could not otherwise be distinguished from hydrodynamic effects, it will be assumed that rotation of the journals about their axes will be zero. If the reference position of the shaft is taken to be in a horizontal plane, the remaining four coordinates could be: (1) vertical displacement of the center of gravity of the journal, (2) horizontal displacement of the center of gravity in a direction normal to the shaft axis, (3) rotation in the horizontal plane about the vertical line through the center of gravity of the journal, and (4) rotation in a vertical plane about the horizontal line which is perpendicular to the shaft axis at its center of gravity. Of these four coordinates, only motion in the first is considered in the initial investigations. Constraints are assumed to prohibit motion in the other three. Later in this paper, angular motion in the coordinate defined by (4) above will also be allowed.

At this point, it seems advisable to give a more-detailed description of the system configuration. The journal being supported is considered to be a solid homogeneous shaft of radius R , length L , and mass m . The bearing which encloses the journal has a length L and a nominal radius $(R+h_0)$. During operation, the bearing radius fluctuates sinusoidally at a high frequency, producing the squeeze effect. The amplitude of this sinusoidal variation is denoted by the symbol h_1 . Assume the

bearing axis and the reference position of the journal axis to lie on the same horizontal line. Then the location of the journal centerline can be specified by a coordinate y measured positive upward from the fixed bearing centerline--this assumes, of course, that the other five coordinates are constrained to be zero as mentioned above. A possible instantaneous configuration of bearing and journal (with the bearing at its nominal radius) is shown in Fig. 1.

Another symbol shown in Fig. 1, but which has not been mentioned previously, is the angle θ , which is measured from the vertical about the centerline of the journal. Since some of the variables to be encountered will be functions of position around the journal, θ is introduced to provide for these functional relationships. These variables will also generally be functions of position along the shaft, so a coordinate z , measured from the left end of the shaft, is provided. The angle θ can assume values between 0 and 2π , while z varies from 0 to L .

The Reynolds Equation

The equation describing the fluid dynamics of laminar gas films is called the Reynolds equation. For a gas bearing in which there is no relative tangential motion between mating surfaces, and for the coordinates θ and z as defined above, the Reynolds equation can be

Fig. 1.--End view of the shaft
indicating nomenclature.

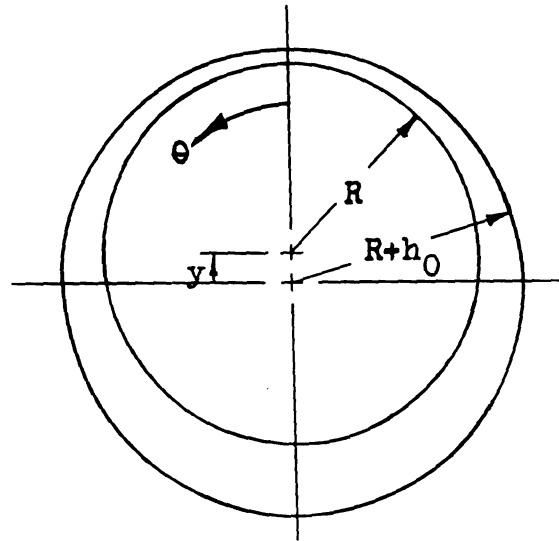
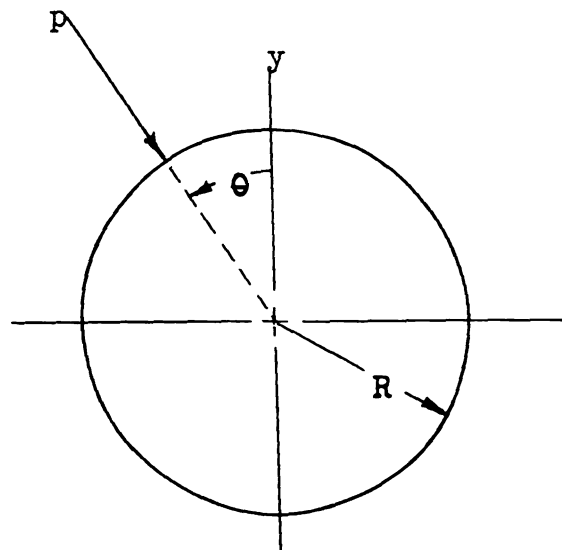


Fig. 2.--End view of the shaft
showing the action of a
general pressure force.



written

$$\frac{\partial}{\partial z} \left[\frac{\rho h^3}{\mu} \frac{\partial p}{\partial z} \right] + \frac{1}{R^2} \frac{\partial}{\partial \theta} \left[\frac{\rho h^3}{\mu} \frac{\partial p}{\partial \theta} \right] = 12 \frac{\partial(\rho h)}{\partial \tau} \quad (1)$$

This equation is readily derived from the general Reynolds equation as given in Gross [12]. In this equation, ρ is the density of the gas film; μ is its viscosity; h is the film thickness at a general location (z, θ) and at a general real time τ ; and p is the pressure at a given (z, θ, τ) .

An assumption which is generally valid in gas bearing work is that the gas film behaves as a perfect gas. Thus, ρ in Eq. (1) can be replaced with

$$\rho = \frac{p}{R T} \quad (2)$$

Another generally-accepted assumption used in gas-bearing work is that the gas behaves isothermally, i.e., T , the temperature, is constant. Also, for an isothermal gas, μ can be considered constant. Then (1) becomes

$$\frac{\partial}{\partial z} \left[p h^3 \frac{\partial p}{\partial z} \right] + \frac{1}{R^2} \frac{\partial}{\partial \theta} \left[p h^3 \frac{\partial p}{\partial \theta} \right] = 12 \mu \frac{\partial(p h)}{\partial \tau} \quad (3)$$

Equation (3) is a relationship containing dimensioned quantities. To make it dimensionless, define $Z=z/B$, where B is some characteristic bearing dimension, and Z is the normalized z ; $P=p/p_a$, where p_a is the ambient pressure, and P is the normalized p ; $H=h/h_0$, where h_0 is the nominal film thickness, and H is normalized h ; and $t=\omega\tau$, where t is normalized time, and ω is some char-

acteristic frequency, usually taken to be the squeeze frequency in squeeze-film work. Using these dimensionless groups, and letting B equal R, (3) can be written

$$\frac{\partial}{\partial Z} \left[PH^3 \frac{\partial P}{\partial Z} \right] + \frac{\partial}{\partial \theta} \left[PH^3 \frac{\partial P}{\partial \theta} \right] = \sigma \frac{\partial(PH)}{\partial t} \quad (4)$$

where the dimensionless constant σ , defined by

$$\sigma = \frac{12\mu\omega R^2}{p_a h_0^2} \quad (5)$$

is commonly called the "squeeze number".

The Equation of Motion

Equation (4) is one of two equations which must be satisfied in order to determine journal bearing stability characteristics. The second is the equation of motion. As stated above, the journal will first be considered free to move in only one coordinate. The forces acting on it are the gas pressure forces, the weight of the journal, and external forces; the last two of these forces are combined in this development.

Figure 2 represents an end view of the journal. The arrow labeled p indicates the pressure applied to the journal at a general location (z, θ) . This pressure applied over an elemental area $Rdzd\theta$ results in a force in the y direction equal to $-pR(\cos\theta)dzd\theta$. The resultant of all such forces is obtained by integrating this elemental force over the complete bearing. Letting the load per unit length, due to the combined effects of shaft weight

and applied forces, be W_1 , the equation of motion can be written

$$\frac{m}{g_0} \frac{d^2 y}{d\tau^2} = - \int_0^{2\pi} \int_0^L R p(\cos\theta) dz d\theta - W_1 L \quad (6)$$

To make (6) dimensionless, use the same substitutions which were used to normalize (3). The resulting equation is

$$\frac{d^2 y}{dt^2} = - \frac{1}{B} \left[\frac{R}{L} \int_0^{2\pi} \int_0^{\frac{L}{R}} P(\cos\theta) dZ d\theta + 2W' \right] \quad (7)$$

where two new dimensionless groups have been used, which are defined as

$$B = \frac{m h_0 \omega^2}{g_0 p_a R L} \quad (8)$$

and

$$W' = \frac{W_1}{2 p_a R} \quad (9)$$

These groups were used previously in Reference [1]. If advantage is taken of the symmetry present in the bearing, both axially and circumferentially, (7) can be written

$$\frac{d^2 y}{dt^2} = - \frac{1}{B} \left[\frac{4R}{L} \int_0^{\pi} \int_0^{\frac{L}{2R}} P(\cos\theta) dZ d\theta + 2W' \right] \quad (10)$$

Determining Stability

The method of determining stability in this inves-

tigation is basically to start the solution of Eq. (10) from a reasonable set of initial conditions and to observe the motion in Y . If this motion is such that the journal "survives" a specified number of squeeze cycles without contacting the bearing, the system is said to have behaved in a stable manner, otherwise unstable.

Since R , L , B , and W' are all known constants for a given case, the solution of (10) would be quite simple except for the presence of P , which is generally a function of position as well as time. Once H is known, it is possible to obtain P from Eq. (4). Referring to Fig. 1 should help to verify that the general expression for h , the dimensioned clearance, can be written

$$h = h_0 - y \cos\theta - h_1 \sin(\omega\tau) \quad (11)$$

This is normalized by using $H=h/h_0$, $Y=y/h_0$, $\epsilon_1=h_1/h_0$, and $\omega\tau=t$, most of which have been used before. The resulting expression for normalized clearance is

$$H = 1 - Y \cos\theta - \epsilon_1 \sin(t) \quad (12)$$

It should now be evident that the general solution of (10) is dependent on both (4) and (12). In a numerical solution of the problem, the system could be given an initial value of Y from which an initial H could be calculated using (12). Equation (9) and this H would yield a P distribution which could be used in (10) to determine a new Y , etc. In theory, this procedure could be continued for as many time steps as desired, but in

practice, the computer time required for repeated solutions of (4) is prohibitive when attempting to obtain a complete stability map. Fortunately, for bearings which operate at high values of squeeze number, a simpler requirement can be developed from equation (4).

Simplified Reynolds Equation for Large σ

Note that Eq. (4) can be rewritten as

$$\frac{1}{\sigma} \left[\frac{\partial}{\partial Z} (PH^3 \frac{\partial P}{\partial Z}) + \frac{\partial}{\partial \theta} (PH^3 \frac{\partial P}{\partial \theta}) \right] = \frac{\partial (PH)}{\partial t} \quad (13)$$

If σ is sufficiently large, this equation can be approximated as

$$\frac{\partial (PH)}{\partial t} \approx 0 \quad (14)$$

or for relatively short times,

$$PH \approx \text{constant in time at any location} \quad (15)$$

Fortunately, for many cases of interest, the numerical values encountered are large enough (10,000 or larger) to make (14) a reasonable approximation. Also, it has been observed [13] that when a bearing is going to become unstable, it generally does so in much less time than would be required for PH to change appreciably. Thus, at least for high squeeze numbers, the use of Eq. (15) in place of the Reynolds equation is a reasonable basis for stability investigations.

A "Mass-Content" Rule

Equation (15) indicates that the product (PH)

should maintain a value which is approximately constant in time at a given location (Z, θ) in the film. This product can, however, assume different values at different locations, i.e.,

$$PH = \Psi(Z, \theta) \quad (16)$$

In order for this reduced Reynolds equation to be helpful in solving (10), it is necessary that the function Ψ be known. One derivation, which was developed by Elrod [14], for an infinitely-long journal with infinite squeeze number and a fixed journal location, resulted in the following relationship:

$$\Psi = \sqrt{1 + \frac{\frac{3}{2}\epsilon_1^2}{1 + \frac{3}{2}\epsilon_2^2}} (1 - \epsilon_2 \cos \theta) \quad (17)$$

Relationships of this type have been called "mass-content" rules, because their derivation is dependent on a consideration of the average amount of mass of the gas contained in the space between bearing and journal.

The constant ϵ_2 in Eq. (17) has not yet been defined. If a bearing operates with a normalized excursion ϵ_1 and supports the journal at steady-state for a given W' , the position of the journal will be a definite average distance below the bearing centerline, i.e., at that location where gas pressure forces just balance W' . In this position, the distance from the bearing centerline to the journal centerline, in normalized form, is

called ϵ_2 , eccentricity.

Equation (17) is not a function of both Z and θ , but is a function only of θ , because the bearing was assumed to be infinitely long. While less-restrictive mass-content rules have been developed and will be discussed later, the stability work done in [1] and much of the work done in the present investigation is based on Eq. (17). Use of this equation was justified initially because it was the best available. Later on, even after a more-accurate rule was developed, (17) was still used to some extent because computer time required to use the new rule was considerably greater. Finally, use of Eq. (17) can be justified because stability plots based on it are not too different from those based on a less-restrictive mass-content rule; where differences do occur, designs based on (17) would be conservative.

Stability of the Infinite Journal

With ψ and H both being independent of Z for infinite bearings, it follows that P will also be independent of Z , and (10) can be reduced to

$$\frac{d^2Y}{dt^2} = -\frac{2}{B} \left[\int_0^\pi P(\cos\theta) d\theta + W' \right] \quad (18)$$

From Equations (12), (16), and (17),

$$P = \frac{\Psi}{H} = \frac{\sqrt{1 + \frac{\frac{3}{2}\epsilon_1^2}{1 + \frac{3}{2}\epsilon_2^2}} (1 - \epsilon_2 \cos \theta)}{1 - Y \cos \theta - \epsilon_1 \sin(t)} \quad (19)$$

Substituting this expression for P into (18) gives

$$\frac{d^2 Y}{dt^2} = - \frac{2}{B} \left[\lambda \int_0^\pi \frac{(1 - \epsilon_2 \cos \theta) \cos \theta d\theta}{1 - Y \cos \theta - \epsilon_1 \sin(t)} + W' \right] \quad (20)$$

where λ has been defined for convenience as

$$\lambda = \sqrt{1 + \frac{\frac{3}{2}\epsilon_1^2}{1 + \frac{3}{2}\epsilon_2^2}} \quad (21)$$

Now the stability characteristics of infinite journal bearings can be determined by solving only this one equation (20) for various values of the system parameters B, ϵ_1 , ϵ_2 , and W'.

Compatible Values of Parameters

In using Eq. (20) to establish stability regions, ϵ_1 , ϵ_2 , and W' cannot all be chosen independently. If any two of them are chosen arbitrarily, there is only one compatible value for the third one. This stems from the fact that the mass-content rule, Eq. (17), was derived from the steady-state Reynolds equation, i.e., the system was assumed to have gone through all transients, so that the only time-variations of any variables were cyclic. If the system is to be in a steady-state configuration, a bearing with an excursion ϵ_1 supporting a

specified W' would support it with a definite average eccentricity ϵ_2 .

Compatible values of ϵ_1 , ϵ_2 , and W' can be determined from Eq. (20) for steady-state. To do this, ϵ_1 and ϵ_2 are specified, and the corresponding values of W' are determined. One way of forcing equation (20) to conform to a set of steady-state conditions at a given ϵ_2 , even for the case of an unstable configuration, is to physically "hold" the journal at $Y = \epsilon_2$ and to let the bearing operate with its excursion ϵ_1 until steady-state conditions are reached. During the transient to reach these steady-state conditions, the bearing is said to be "pumping up". The transient itself could be followed by solving the Reynolds equation. This has been done in [13] for infinitely-long flat-plate squeeze-film bearings. Also, the steady-state pressure distributions for parallel flat discs have been predicted for various cases in Ref. [10]; some of these cases were confirmed experimentally. The results of both of these papers show that the bearing actually does pump up, with the average final pressure in the film being higher than ambient.

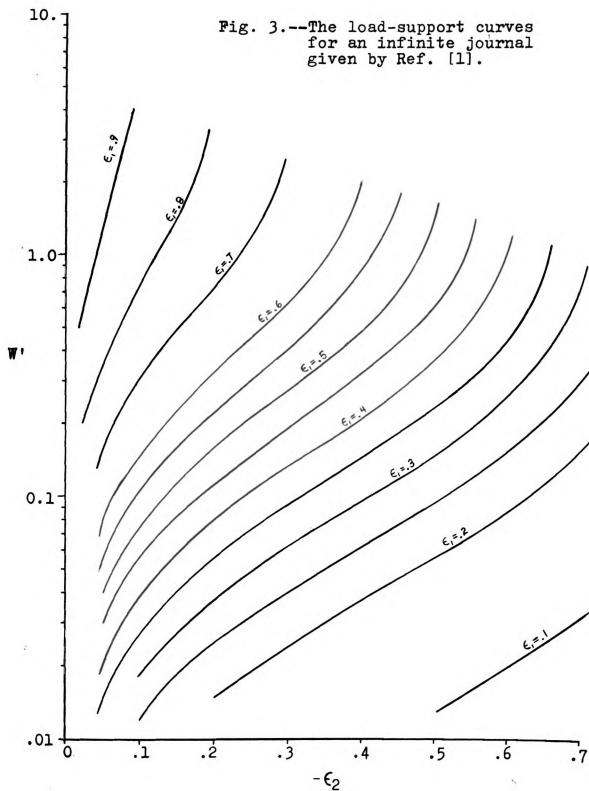
If the journal is held in the $Y = \epsilon_2$ position, Eq. (20) can be averaged in time to give

$$W' = - \frac{\lambda}{2\pi} \int_0^\pi \int_0^{2\pi} \frac{(1 - \epsilon_2 \cos\theta) \cos\theta d\theta}{1 - \epsilon_2 \cos\theta - \epsilon_1 \sin(\tau)} dt d\theta \quad (22)$$

This expression was used in Ref. [1] to establish the family of curves shown in Fig. 3. In the present investigation, a more-extensive set of these curves was required, so a computer program called COMPAT was written which solved Eq. (22) for many more possible combinations of ϵ_1 and ϵ_2 . The results of COMPAT were not plotted, but values were taken from the computer print-out as needed. Plots of the type shown in Fig. 3 are called "load-support curves".

Solution of the Equation of Motion

The procedure for testing the stability of a bearing for a given set of operating conditions can be outlined as follows. First, choose values of ϵ_1 , ϵ_2 , and W' which are compatible with Eq. (22). Then, assume that the journal is held at $Y = \epsilon_2$ while the bearing is operated with an excursion ϵ_1 until it pumps up to steady-state. When steady-state is reached, Eq. (22) should be satisfied, and the average of the resultant of the pressure forces should just balance W' . Then, if the constraint which was holding the journal at its equilibrium position is removed, (20) becomes the governing equation. It is the solution of this equation that is the basis of stability in the method of analysis



used. If the motion in Y is such that it would cause the journal to contact the bearing, the system is said to be unstable, otherwise stable.

An explicit expression for $Y(t)$ satisfying Eq. (20) appeared to be very difficult to derive, because the equation is nonlinear. Thus, it was decided to solve this equation by finite-difference methods. The method of solution used considers (20) to be a special case of the more-general form

$$\frac{d^2 Y}{dt^2} = f(t) \quad (23)$$

The initial value of Y is specified; it may or may not equal ϵ_2 , depending on whether it is desired to start the journal from equilibrium or from some distance away from equilibrium. Both types of starts are considered below; in any case, the initial value of Y is called Y_0 .

Subsequent values of Y are determined at time intervals Δt . The value of $Y(\Delta t)$ can be approximated by a Taylor series:

$$Y_1 = Y(\Delta t) = Y(0) + Y'(0)\Delta t + \frac{Y''(0)}{2}(\Delta t)^2 + \dots \quad (24)$$

Assuming that the journal is released from rest, $Y'(0)$ equals zero, and, from (23), $Y''(0) = f(0)$, so (27) becomes

$$Y_1 = Y_0 + \frac{f(0)}{2}(\Delta t)^2 \quad (25)$$

For Y_2 , the following approximation can be used:

$$Y_2 = 2Y_1 - Y_0 + (\Delta t)^2 f_1, \quad (26)$$

and the remaining values of Y can be calculated from the general expression

$$Y_m = 2Y_{m-1} - Y_{m-2} + \frac{(\Delta t)^2}{12} [13f_{m-1} - 2f_{m-2} + f_{m-3}] \quad (27)$$

This last approximation is given in Crandall [15], and it is accurate to the order of $(\Delta t)^5$.

In using this finite-difference technique to solve Eq. (20), it is obviously not feasible to allow the tests to go on indefinitely in time. Instead, the computer runs have been limited to a specified number of cycles. The "unstable" points determined by this method actually are unstable, since they were tested over a sufficient number of cycles for the instability to occur. The "stable" points, however, left room for doubt, since such a point might have gone unstable if allowed even one more time step. In order to remove some of this doubt, especially in the earlier runs, plots of Y versus t were obtained. The unstable points generally went unstable in a fraction of the number of cycles allotted, by oscillating with increasing amplitude. The plots for the stable points survived the number of cycles allotted, generally following one of two patterns: either oscillations of nearly constant amplitude, or oscillations with an oscillating amplitude (beating). In most cases, the repetitious nature of the response was apparent, and it

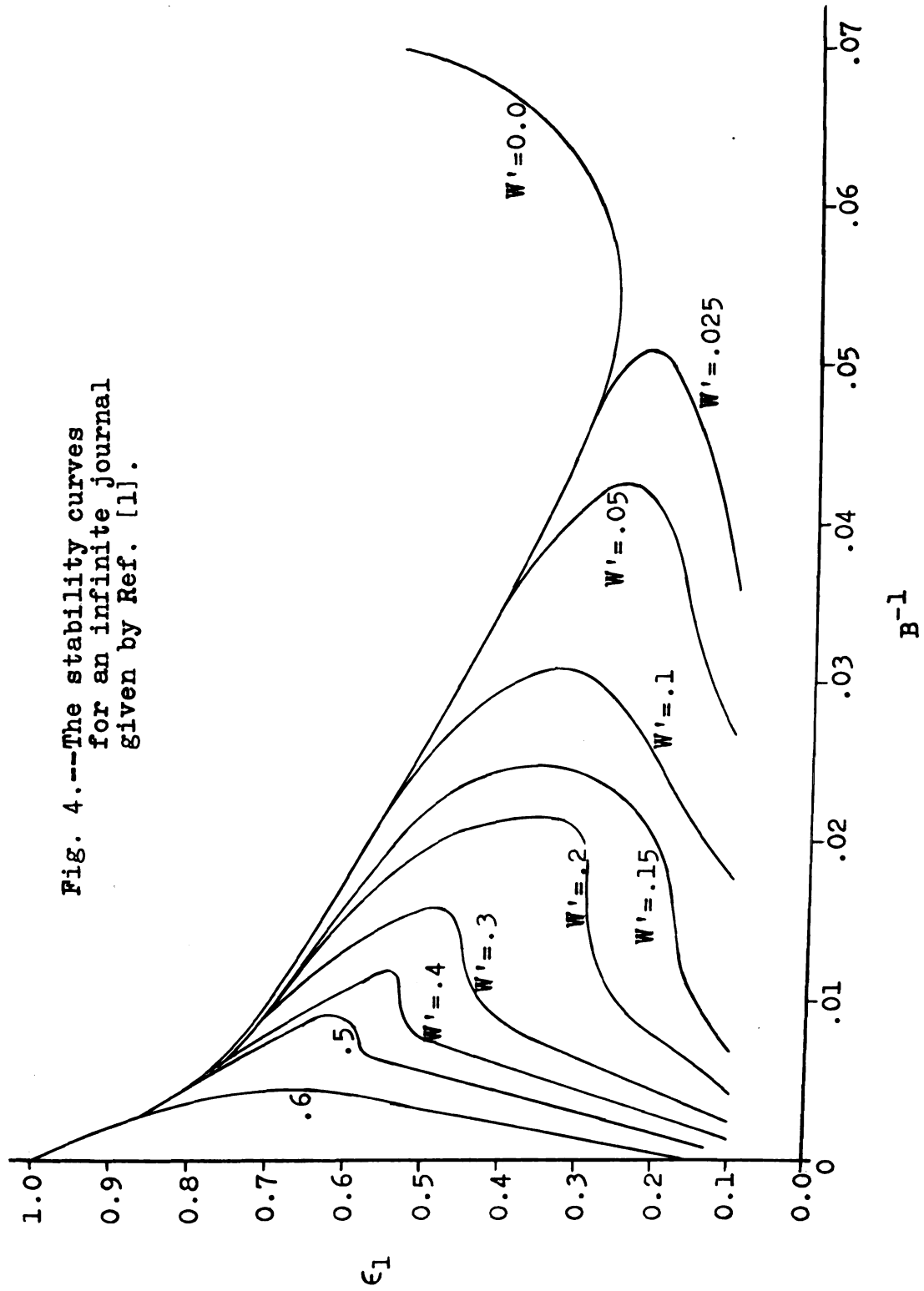
was this apparent good behavior which justified the method used. A few so-called "spongy" regions appeared, in which the "unstable" points ran for almost as many cycles as the "stable" points, but, since these regions generally appeared in less-critical parts of the stability map, they were not retested with more allowable time steps. Some typical response plots will be discussed later in more detail.

The Results of Beck and Strodman

The first family of stability curves for infinite journal bearings was derived by Beck and Strodman [1]. In this work, the boundaries between stable and unstable regions for given values of W' were plotted with ϵ_1 as the ordinate and B^{-1} as the abscissa. The complete family of curves for a range of parameters was plotted and is reproduced in Fig. 4. The region of unstable points for a given W' is the area to the left of the curve for that W' ; the region of stable points is to the right.

In locating these curves, the finite-difference method just discussed was used, with eighty cycles of squeeze required for stability. The method of searching for the boundary was: (1) to hold both W' and ϵ_1 constant, (2) to begin with a value of B^{-1} in the unstable region (which was predicted approximately by a small-parameter analysis leading to a form of the Mathieu equa-

Fig. 4.---The stability curves
for an infinite journal
given by Ref. [1].



tion), and (3) to decrease B^{-1} in steps until a stable point was found. Then a new value of ϵ_1 was read in, and the process was repeated until enough boundary points were located to outline a curve for that value of W' . There is a definite drawback to this method of searching, namely that boundary points could be located only if they could be "seen" from the starting point for a given ϵ_1 . The search was conducted on a constant- ϵ_1 straight line, and there was no provision for turning corners if any should exist. The need for the ability to turn corners did not become apparent until Strodtman, in attempting to verify the results of Fig. 4 with an analog computer, observed unstable behavior at certain points within the "stable" regions. Some of these same points were tested by the original method, allowing 250 cycles for stability, and they also went unstable by this method. It was decided that there must be some type of "holes" in the stable regions, but not enough points had been tested to completely define the nature of these holes. While points in the vicinity of the holes could have been tested at random until the boundary could be sighted-in between the stable and unstable fields of points, this would have required much computer time, with 250 cycles being allowed, and also many runs in order for the investigator to be able to determine which points to try next. It seemed that what was needed was a computer program

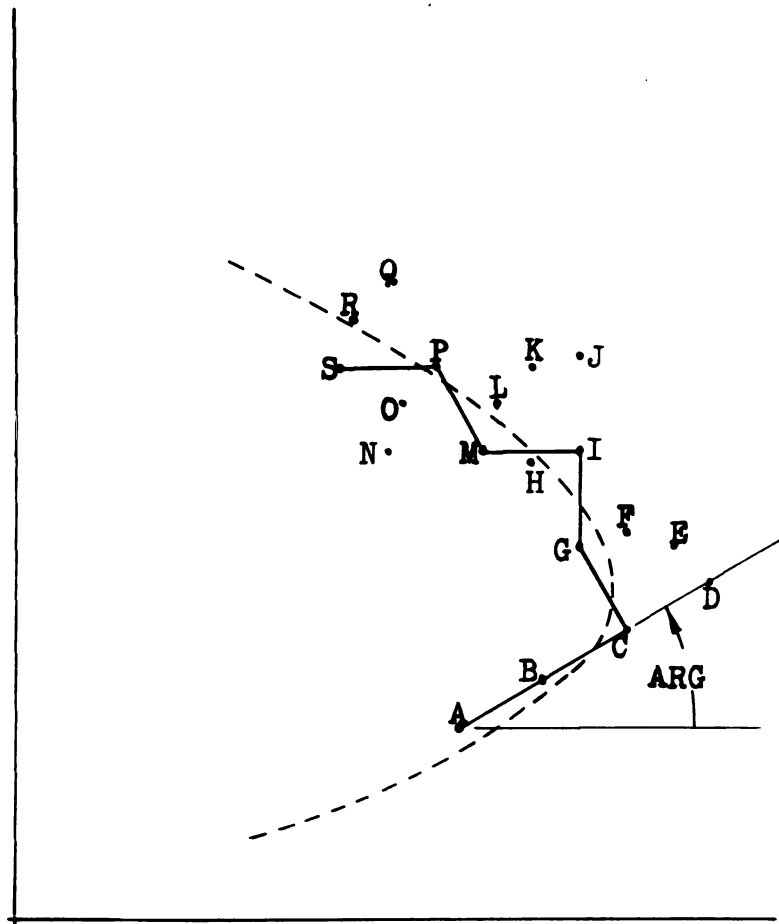
which could locate and follow a stability boundary, even around sharp corners, without having to test an excessive number of points. The development of such a method of analysis is one of the prime contributions of the present investigation.

The "Automatic" Program

In the initial search for a program which would automatically locate and follow a stability boundary, many possible methods were considered. Each proposed logic was applied graphically by hand to a typical section of curve which contained a sharp bend. None of the methods failed to trace out a reasonable approximation to the gradually-curved part of the plot, but the abilities of the methods to negotiate the sharp turn varied considerably; many of the methods would not follow the turn at all.

The method which was finally adopted can best be explained by considering a graphical application of it to a specific curve. Let the boundary of interest be represented by the curve of Fig. 5. This method begins by locating two points just inside the stable region, using a method similar to that of [1]. These first two points are labeled A and B in the figure. After A and B are located, it is required that all succeeding points on the approximate curve alternate in-and-out of the unstable region and that each point be a known small distance

Fig. 5.--Graphical presentation of the automatic seeking method.



(called DIST in the computer programs) from each of its two neighbors. These two requirements force all points on the approximate curve to fall no further than DIST from the true curve.

Points A and B define a straight line which is directed at an angle ARG to the horizontal as shown. The next trial point is located by extending a distance DIST from B in the direction of ARG. Since this new point, C, is in the unstable region, it will be the next point on the approximate boundary. If C had fallen in the stable region, ARG would have been decreased by a given angle DELARG, and the process would have been repeated until the trial point did fall in the unstable region. Note that, for this procedure to work, B must be no further than DIST from the true boundary.

Following this procedure, the next trial point, D, is located by extending a distance DIST from C in the direction of ARG. Since C was in the unstable region, the next good point should be in the stable region. Thus, D is discarded, ARG is increased by DELARG, and the next trial point, E, is located from C a distance DIST in the direction of the new ARG. This procedure is repeated until the next stable point is found, and the general procedure continues, locating alternating stable and unstable boundary points, until the complete curve is traced.

The above method is the basis of all the automatic

techniques used in any of the computer runs. However, many modifications were made to overcome specific difficulties which occurred. In particular, at least eight different starting procedures were used, to accomodate starting from the unstable region and moving up; starting from the unstable region and moving down; starting in a hole, moving left and up; starting in a hole, moving left and down; etc. Also, as various corners were encountered which could not be followed, the computer logic was modified accordingly. These modifications were suggested as a result of manually plotting what path the computer was following and determining what a new logic must include in order to avoid the same difficulty. Although it is possible to sketch curves which the best of these methods cannot follow, fortunately no such curves have been encountered in the stability plots studied. The curve-following logic from one of the more-effective programs is discussed in more detail in Appendix A.

It should be obvious from the geometry of the method that smaller values of DIST result in a better reproduction of the desired curve, but also require that a greater number of points be tested. While small values of DELARG may allow the method to progress quite efficiently along relatively-straight portions of the curve, larger values allow it to turn corners more quickly. It

was decided on the basis of some manual applications of the method that a DELARG of fifteen degrees (.261799388 radians) gave reasonable accuracy and speed over either straight or curved sections of curve. Although the programs provided for reading in DELARG with each new set of data, this same value was used throughout. DIST was given different values depending on the detail expected in the region being tested. In all cases, the value of DIST used was specified in terms of the ordinate scale of the curve being traced, e.g., if DIST is given as 0.025, and if one inch on the ordinate represents 0.1 units of the ordinate variable, then DIST would be one-fourth inch on that plot.

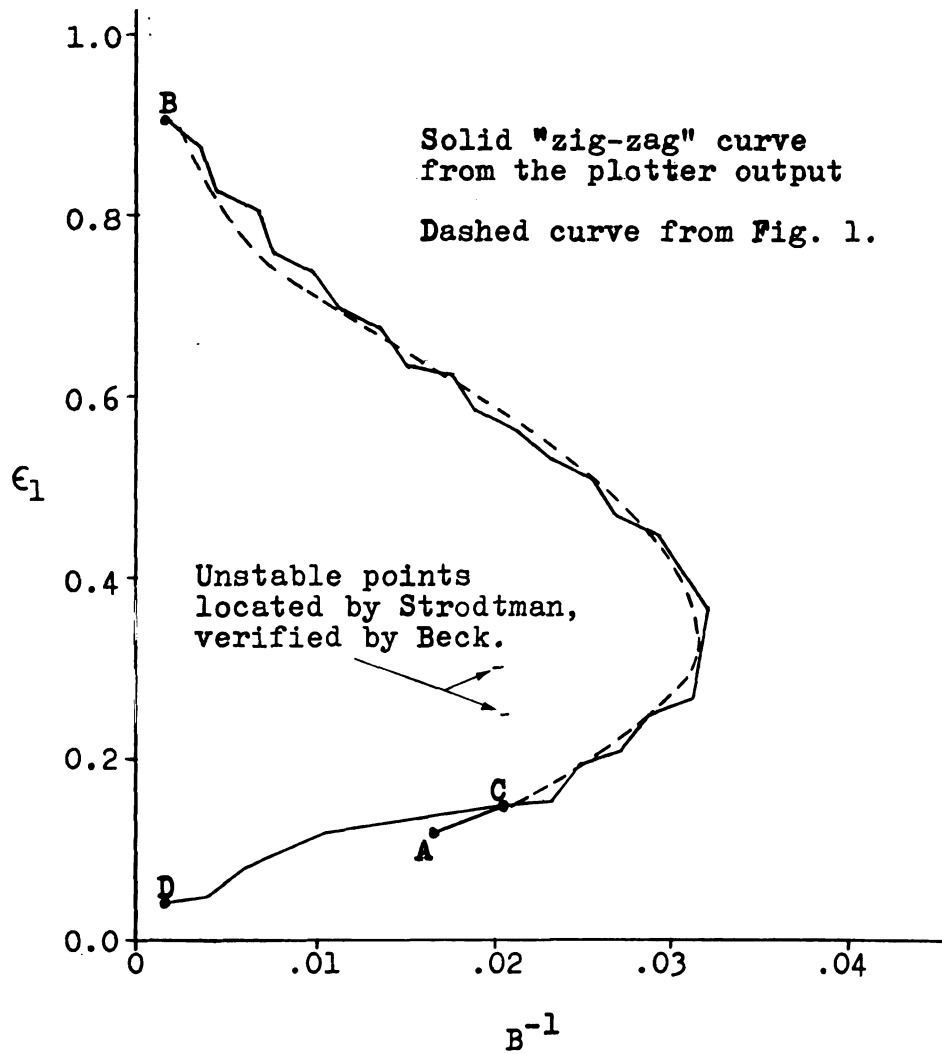
The first automatic programs were used to follow curves similar to those given in Fig. 4, i.e., plots of ϵ_1 versus B^{-1} at constant W' . In methods used before the automatic programs were developed, it was known in advance what the values of W' and ϵ_1 of the tested points would be, and so the corresponding value of ϵ_2 , to satisfy Eq. (22), could be read into the program as data. In the new programs, the order in which points would be tested could not be predicted; thus there was a need in the program for a means of calculating compatible values of ϵ_2 for given values of ϵ_1 and W' at each point. Since each curve was to be plotted for a constant W' , this problem was solved by reading in a complete range of com-

patible values of ϵ_1 and ϵ_2 for this W' , and then interpolating for the ϵ_2 values as the corresponding values of ϵ_1 became known. This method worked very well for the problems involving Elrod's mass-content rule, but it will be demonstrated that it could not be used practically with the more-accurate mass-content rule developed by Beck.

Finding the "Hole" Automatically

It has been stated that a few unstable points had been located inside the "stable" regions given in Ref. [1]. Specifically, some of these points occurred inside the plot for $W' = 0.1$ at the locations shown in Fig. 6. The information given by these few points was not sufficient to tell whether the hole was closed inside the stable region or whether it might open out into the larger unstable region. If this latter possibility had been the case, it should have been possible to locate the hole by following the original stability boundary into it. Thus the first automatic programs were used in an attempt to locate the hole in this manner. The first of these programs was started at point A of Fig. 6 and allowed to follow the boundary upward to point B. The zig-zag pattern shown was taken directly from the plotter output; it is so coarse because DIST was specified as 0.050. Since this run failed to locate the entrance to the hole, the program was modified so that it would start at point C

Fig. 6.--The first stability plot
from an automatic program;
for $W'=0.1$.

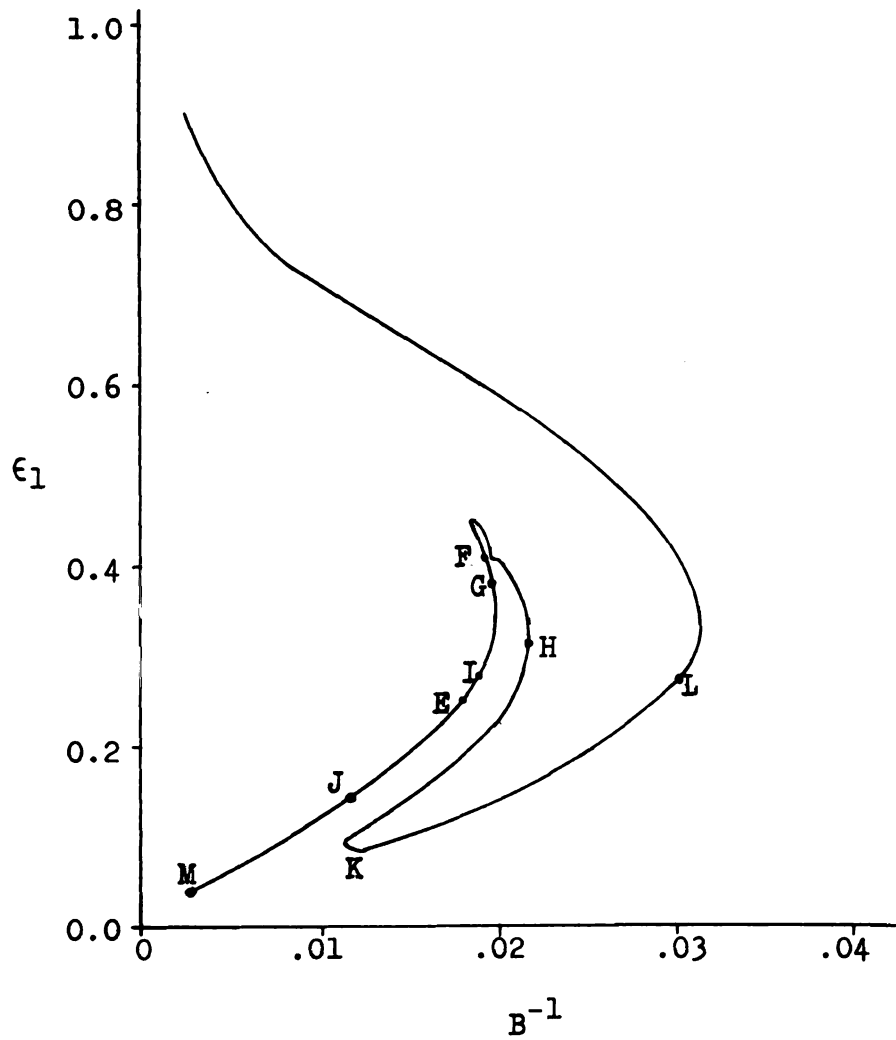


and work downward. The computer plot of this run is represented by the line C-D. This run did not locate the entrance to the hole either, although it was discovered later that it should have; the start-up procedure was so coarse that it jumped over the entrance.

At this point in the investigation, it was believed that the hole did not open out into the large unstable region, so a program was developed which would start from inside the hole. While the two runs from A to B and C to D were allowed fifty cycles for stability, 250 cycles were allowed for runs inside the hole. Also, DIST was reduced to 0.01, since it was anticipated that features inside the hole would be somewhat finer than those on the outside. Both of these changes obviously increased the computer time required to progress a given distance, but, for this test case, it was felt to be justified.

The curve from E to F in Fig. 7 represents the first section of boundary located inside the hole. The next run began at point G and ended at H. This was the first relatively-sharp turn that was followed by any of the programs. The next run gave the points from I to J, and it was expected that a run started downward from point H, if given enough time, would eventually close the hole. When this was tried, however, the curve did not close, but instead doubled back around point K to point L. The last section tested was from J to M; here the

Fig. 7.--Stability plot for $W'=0.1$, showing detailed construction of the hole.



program stopped, because the value of ϵ_1 at point M was the lowest value which could support a W' of 0.1. Thus, it was finally shown that the hole did open out through the bottom of the original stability region.

The total computer time used for the portion of Fig. 7 from M to L was approximately 45 minutes on the CDC 3600. The reason for this, as suggested earlier, is that the tested points in this region were very close together and that 250 cycles were required for stability. While such a time-consuming method might be justifiable for a test case, it would obviously not be practical to obtain a complete family of curves in this manner. However, before the next modification of the method is discussed, it is interesting to compare plots of $Y(t)$ for some of the points tested in obtaining Fig. 7.

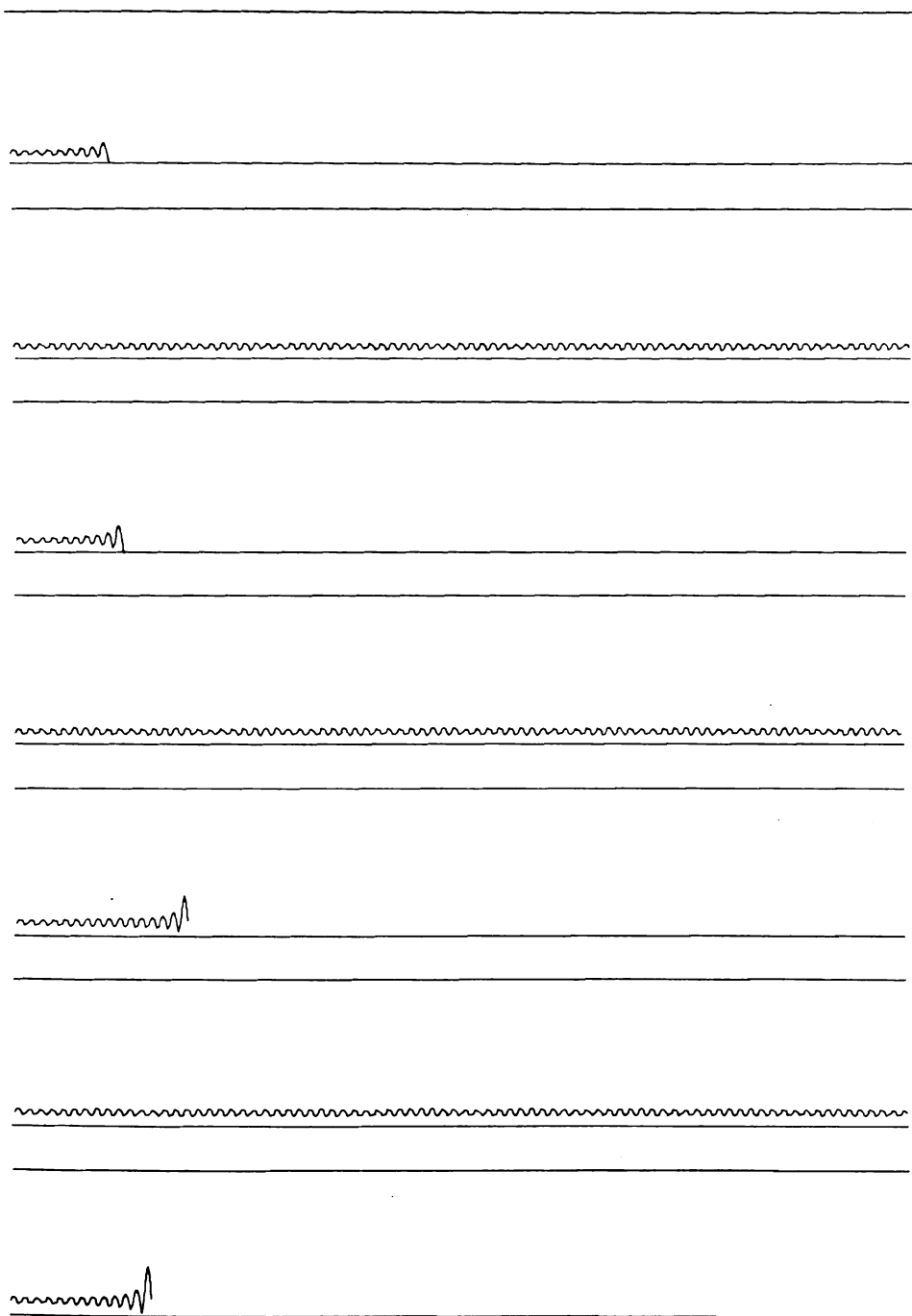
Comparison of Some Y Responses

It has been emphasized that whether a point of operation is called stable or unstable depends on whether or not the journal can survive a specified number of squeeze cycles without contacting the bearing wall. The method may be questioned in that survival of the specified number of cycles gives no assurance that the bearing will remain stable for all time; the journal could conceivably hit the wall in the very next time step after the last one tested. It is not necessary to run the cases for longer times, because plots of the response Y as a

function of t show trends of the responses near the point of cutoff. Typical examples of these response plots are shown in Figures 8 through 10. For each case represented, there are two straight lines with the Y plot in between. The straight lines represent the innermost positions of the upper and lower bearing walls, i.e., they are located at a distance $(1-\epsilon_1)$ above and below the bearing centerline. If the plot of Y ever crosses either of these lines, collision of the journal and bearing is indicated, and the case is called unstable (Because the subroutine used to plot these curves did not plot the last point tested, many of the plots fail to cross either boundary. However, any case for which the plot is cut off prematurely is unstable.) Note that the radius of the journal is neglected in these plots. The full abscissa scale in all cases represents 250 cycles of squeeze. All runs were started with $Y_0 = \epsilon_2$, i.e., from the equilibrium position.

Figure 8 shows the plots for some representative points in the vicinity of point J of Fig. 7. These response plots are for consecutive points near J which alternate in-and-out of the stable region. Since the value of DIST used in all of these runs was 0.01, neighboring stable and unstable points are very close together; yet there is a marked difference in their response plots. The unstable responses of Fig. 8 terminate in relatively

Fig. 8.--Typical response plots for points in
the vicinity of point J of Fig. 7.



few cycles, while the repetitive nature of the stable responses suggests that they would remain stable even beyond the point of cutoff. Thus, the method of analysis seems to have defined the stability boundary quite well in the vicinity of point J. Note that some slight beating is apparent in the stable responses.

Response plots from point J up through point G of Fig. 7 showed generally the same tendencies as those shown in Fig. 8, i.e., the unstable points showed their instability quickly, while the stable points showed no tendency to become unstable. There was, however, a general trend of the unstable points to require more cycles to become unstable as point G was approached.

From point G around the bend to point H, the conclusions to be made from the response plots were not nearly so definite. This is the so-called "spongy region" which was mentioned earlier. Response plots for all of the points tested through this region are shown in the three pages of Fig. 9. Note that the consecutive response plots are numbered from the bottom up; this is the way that they came from the plotter. Note the uncertainty presented in this series of plots. Some of the unstable points survived many more cycles than previously. Unpredictable beating occurred which sometimes carried the bearing into instability and sometimes allowed it to pass the 250 cycles while leaving doubt that it

Fig. 9.--Typical response plots for points
from point G to point H of Fig. 7.

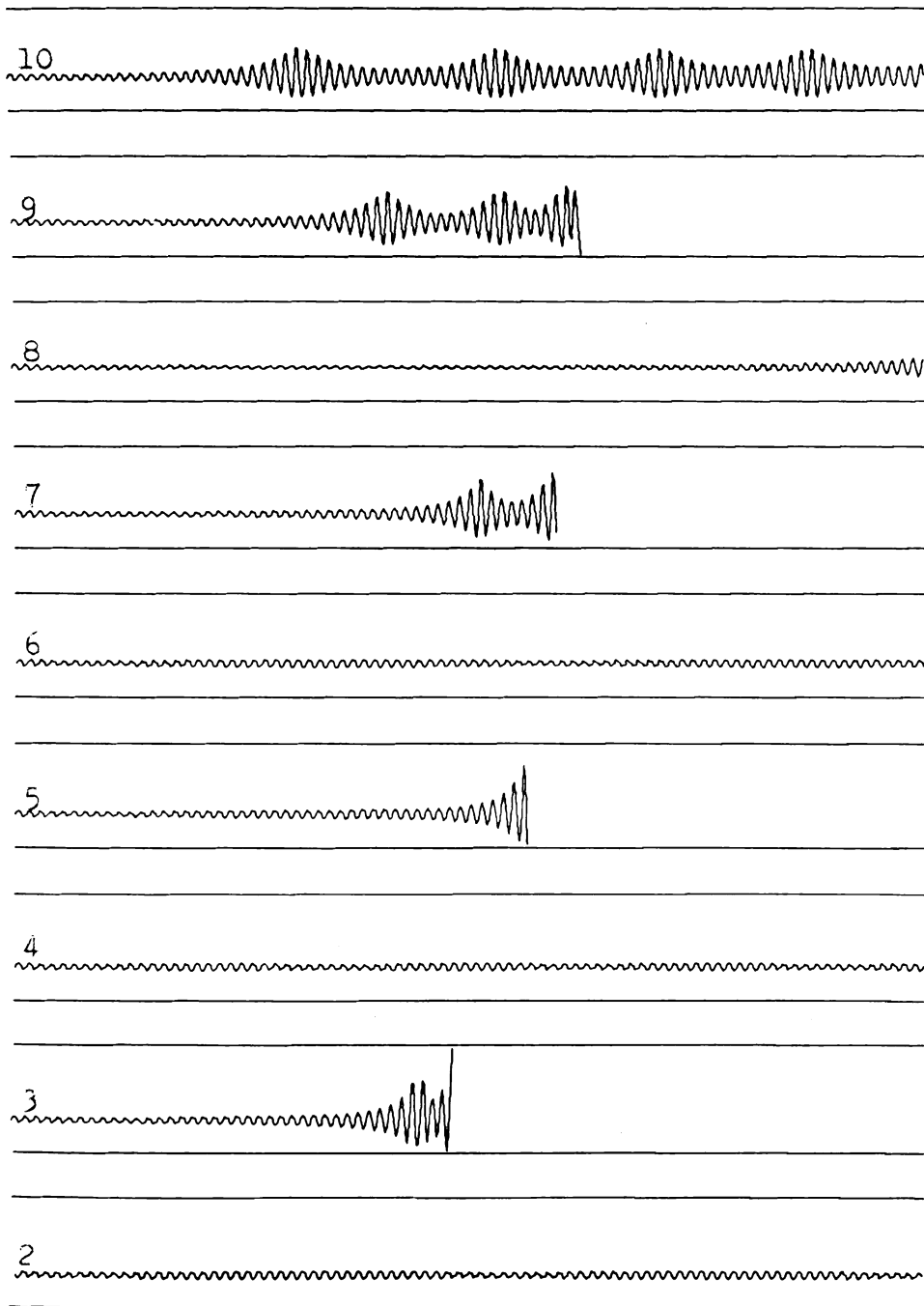


Fig. 9.--(Continued)

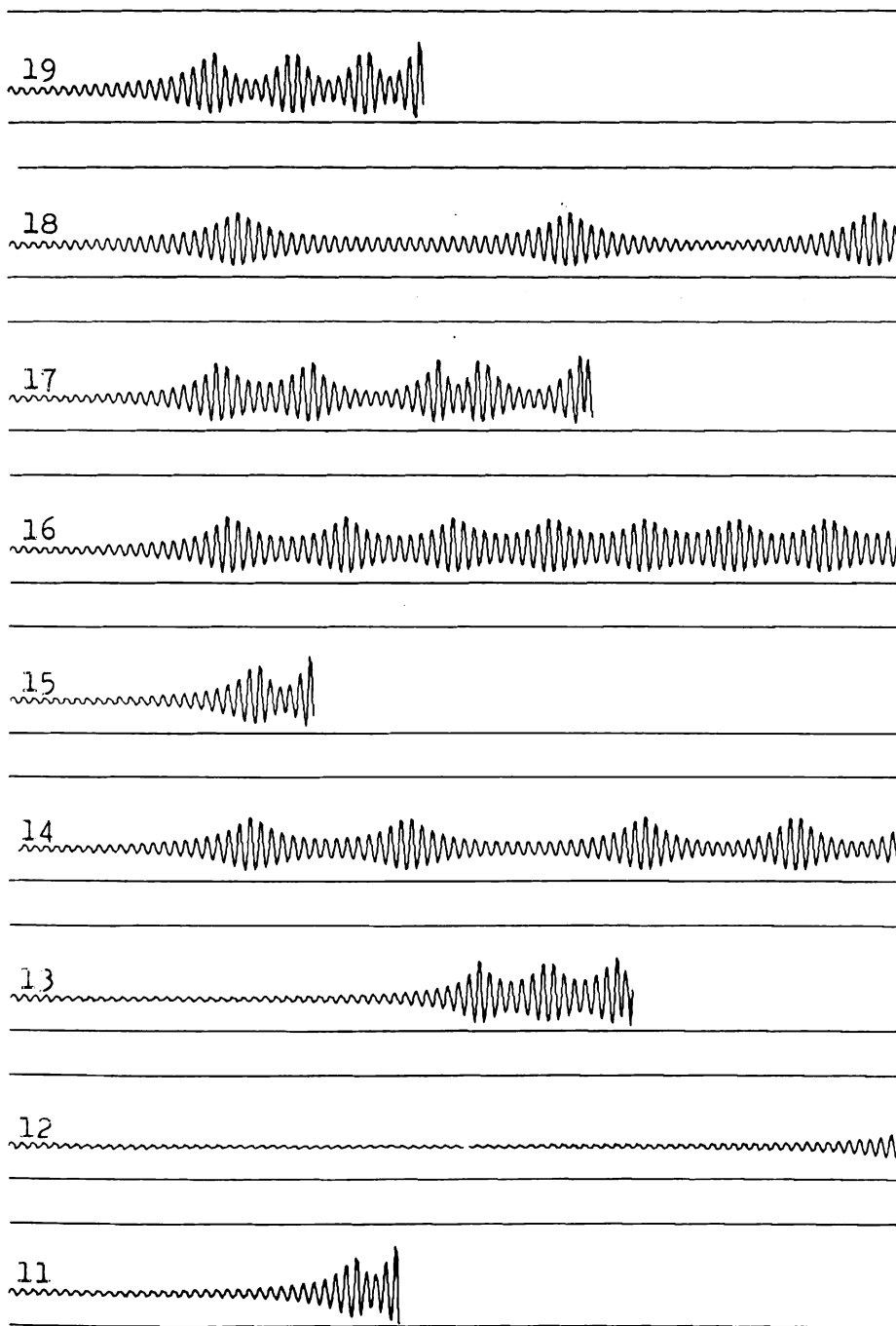
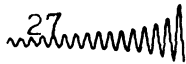


Fig. 9.--(Continued)

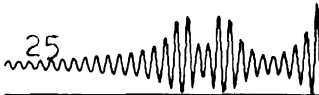
27



26



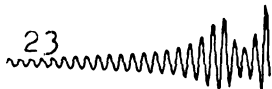
25



24



23



22



21



20



should be stable there. Plot number 8 of Fig. 9 represents the highest point tested on the hole boundary. This response is quite well-behaved for most of the allotted time, but it is growing steadily in amplitude near the point of cutoff, and thus should no doubt have been labeled unstable; the same can be said for plot 12.

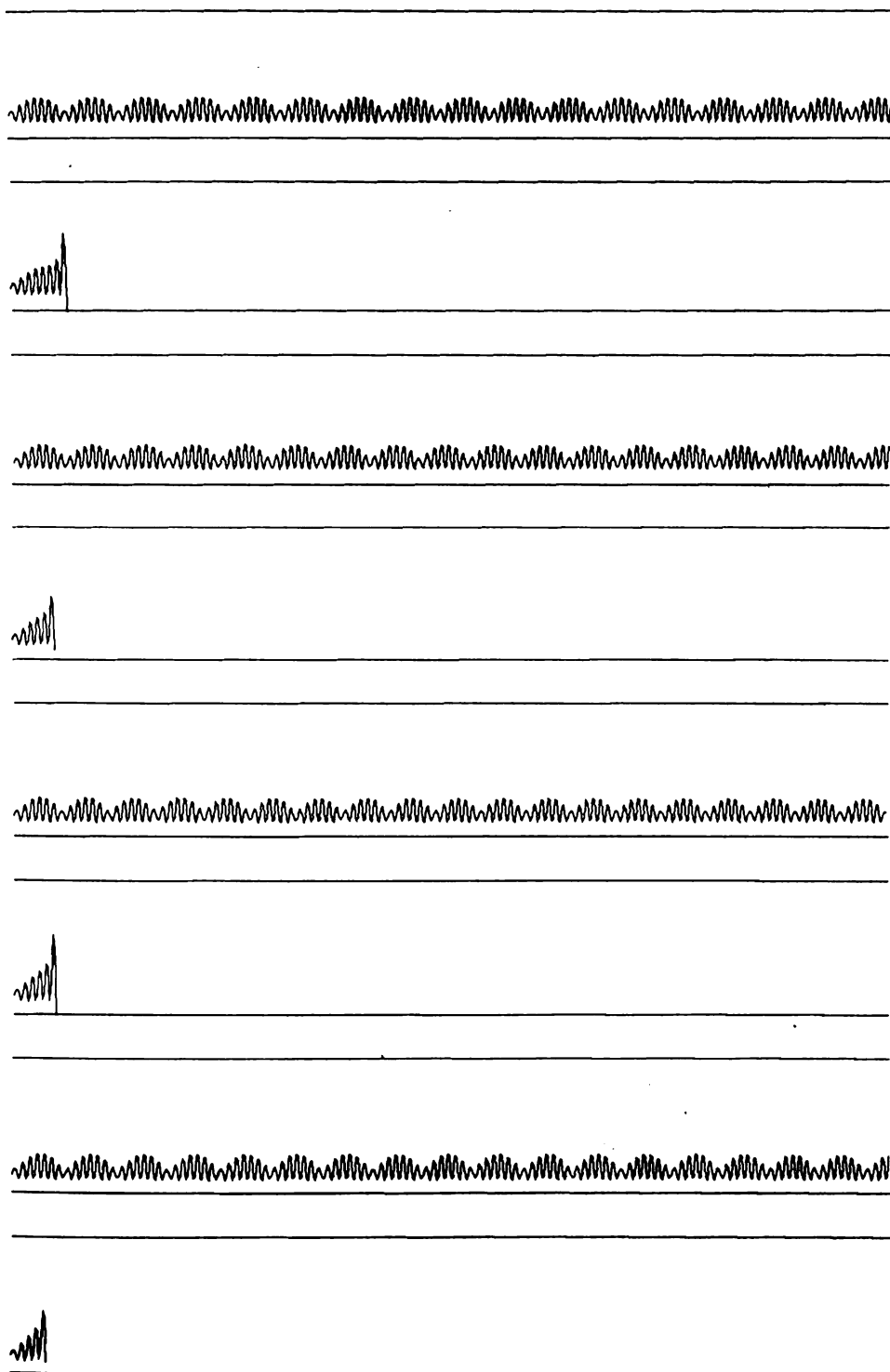
Fortunately, the "spongy" region appeared only near the top of the hole. As other points were tested from point H to point L of Fig. 7, the responses resumed a nature similar to those which were exhibited from point J to point G. The unstable points went unstable in very few cycles and without any beating; the stable points showed beating which became more apparent as point L was approached, but there was no indication that the bearing would go unstable at these points. Typical plots for the region around point L of Fig. 7 are shown in Fig. 10. Note how the lower extreme of motion in Y for the stable plots is relatively constant, while the beating appears to all occur on the upper amplitude.

Except possibly in the relatively small "spongy" region, it is felt that the method being used to determine stability leads to reasonably-accurate stability plots. Thus, the same basic method is used throughout this investigation.

Speeding-up the Process

After establishing the complete stability plot, in-

Fig. 10.--Typical response plots for points in
the vicinity of point L of Fig. 7.



cluding the hole, for $W' = 0.1$, it was desired to apply automatic programs to plots for the other values of W' tested in [1] in hopes of locating holes in these as well. As mentioned before, however, to trace the complete family of curves with the same accuracy as used in following Fig. 7 would be too consuming of computer time. The case of $W' = 0.1$ was a pilot case, and thus it was felt justifiable to make it more accurate than might be necessary; then it could be used as a standard to compare with when coarser methods were used.

One means of reducing the computer time necessary to run a stability curve is to test fewer points by increasing DIST. The obvious disadvantage in this is that fine variations in the curve might be missed, but the distance used in obtaining Fig. 7 was probably finer than necessary. Thus, in most of the remaining runs, a DIST of 0.025 was used.

A second possible means of saving computer time would be to use fewer time steps per cycle in the approximate solution of Eq. (20). While forty time steps per cycle were used in obtaining Fig. 7, it is concluded below that ten gives reasonable accuracy.

Reducing the number of squeeze cycles used as the criterion for stability would also speed up the process. However, since many of the unstable points, especially inside the hole, of Fig. 7 took almost the allotted 250

cycles of squeeze to go unstable, it is likely that reducing the number of cycles would reduce the size of the hole or even cause it to be missed completely. The number of cycles might be reduced if some means could be devised to cause the instabilities to become apparent in a fewer number of cycles. All of the cases tested up to this point had been started with the journal at $Y_0 = \epsilon_2$, the equilibrium position predicted by Eq. (22). It seemed reasonable to expect that starting the journal with a Y_0 somewhat displaced from equilibrium might hasten the onset of instability for unstable cases. There was also the possibility that this procedure might result in some of the stable points becoming unstable, but it appeared to be worth investigating.

The new expression for Y_0 incorporated into the computer program was based on the equation

$$Y_0 = \epsilon_2 - \text{CRD}(1 - \epsilon_1 + \epsilon_2) \quad (28)$$

where CRD is a constant which can be given any value between zero and unity. If CRD = 0, $Y_0 = \epsilon_2$, the same as before. If CRD = 1, $Y_0 = (-1 + \epsilon_1)$, which would mean that the pulsating bearing would just contact the bottom of the journal on its inward strokes. If the journal is at $Y = \epsilon_2$ and the bearing excursion is ϵ_1 , the minimum clearance between the journal and bearing is $(1 - \epsilon_1 + \epsilon_2)$. Thus, CRD is the fraction of this minimum clearance that the journal is displaced from equilibrium before being

released.

The first stability plot made using the above-mentioned modifications is shown in Fig. 11 superimposed over a reproduction of the plot of Fig. 7. The value of CRD used in obtaining this new plot was 0.5, and only fifty cycles were taken as the basis of stability. The approximate solution was based on ten time steps per cycle of squeeze. The hole is quite apparent in this figure. Starting with such a high value of CRD not only located the hole; it also caused some points which were stable in Fig. 7 to be in the unstable region here. It should be clear that a bearing which inherently tends to keep its journal near the equilibrium position (i.e., be stable) can be caused to exhibit unstable behavior by choosing an extreme set of starting conditions. In proposing the method involving CRD, it was not intended that the stability plot of Fig. 7 for $W' = 0.1$ be changed; it was only hoped that a value of CRD could be found which would cause unstable points to go unstable quicker, but still not cause any previously-stable points to become unstable. Thus, a CRD of 0.5 is too large.

The second value of CRD to be tried was 0.25. Ten time steps per cycle were also used in this run. The resultant plot is given in Fig. 12 along with a reproduction of the desired plot. Note that, as expected, the hole is smaller than it was for $CRD = 0.5$, and that this

Fig. 11.--Stability plot for $W'=0.1$, $CRD=0.5$,
superimposed over the plot of Fig. 7.

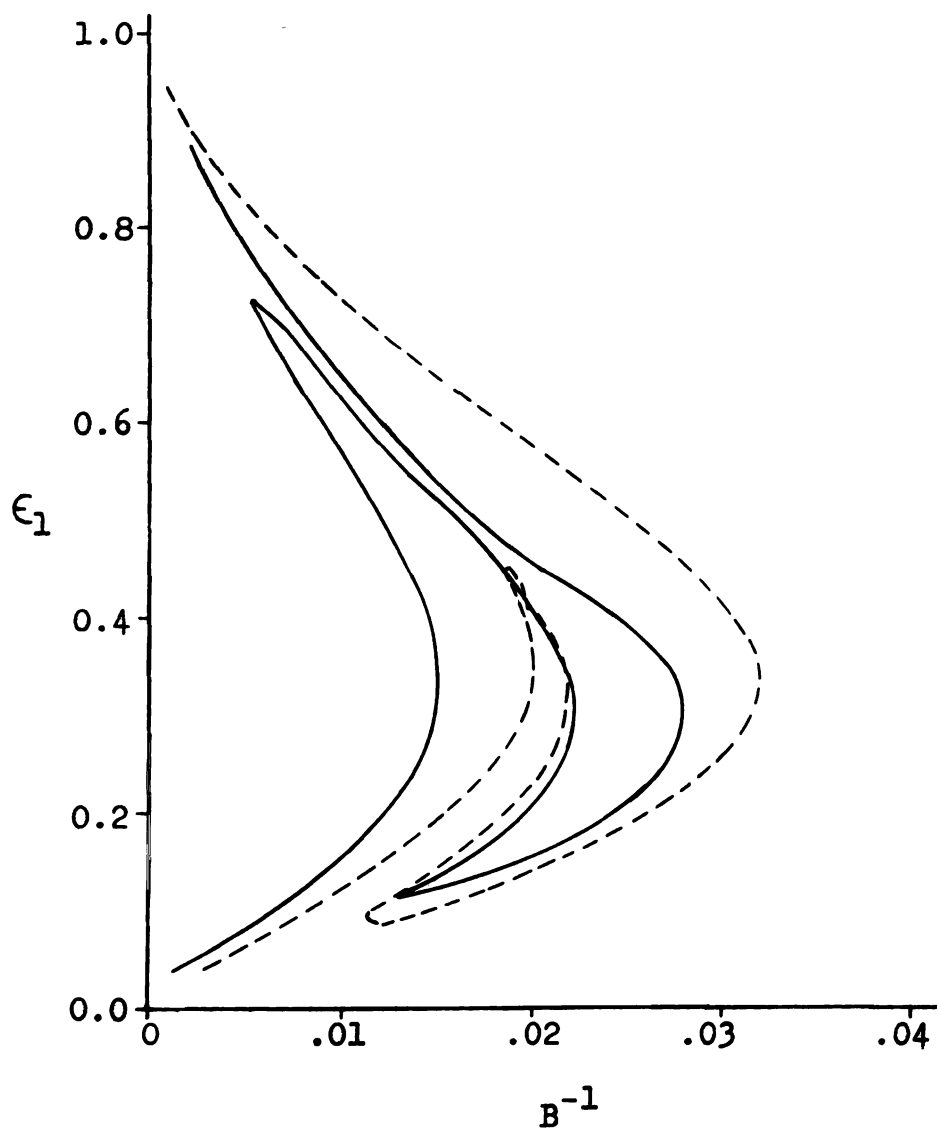
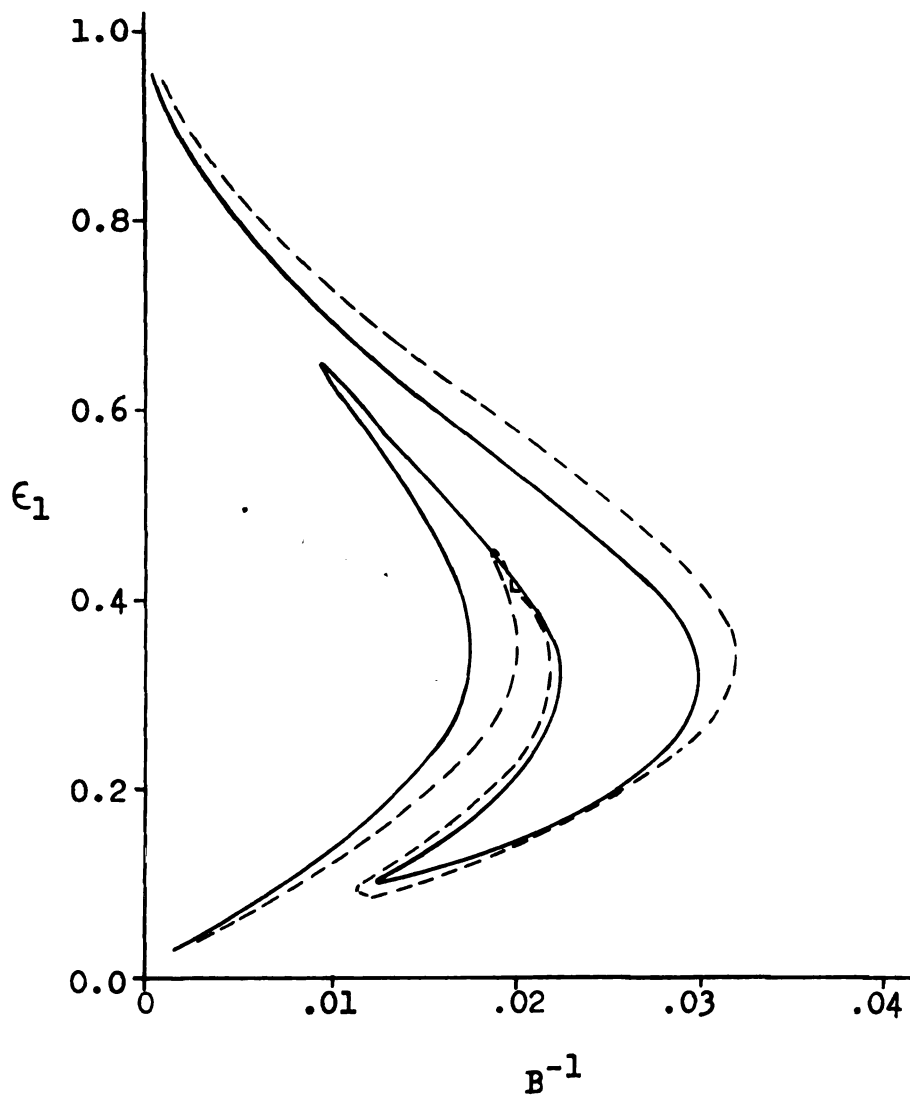


Fig. 12.--Stability plot for $W'=0.1$, $CRD=0.25$,
superimposed over the plot of Fig. 7.

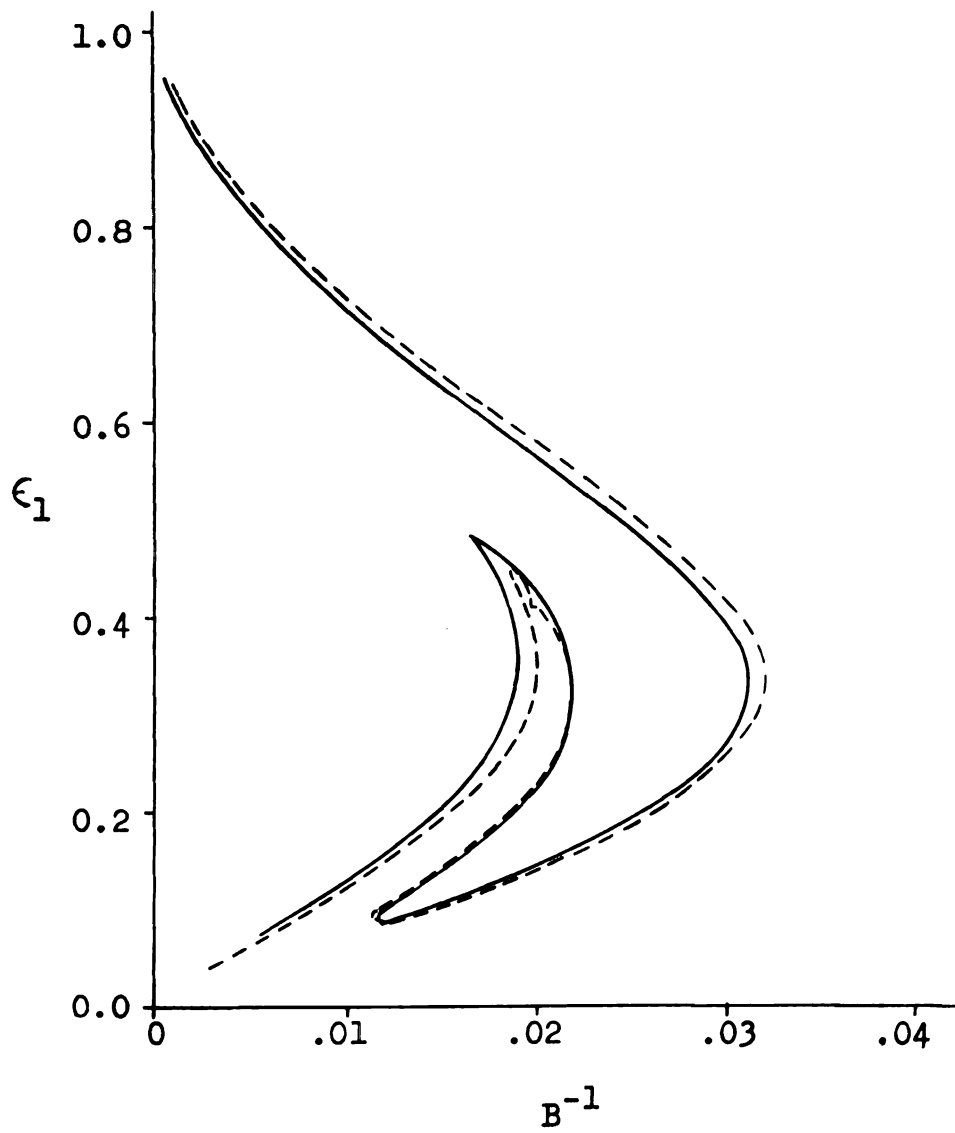


plot is generally a better approximation to the desired plot. It is interesting to note in both Figs. 11 and 12 that the stable region is only affected on the left side of its neighboring unstable region, i.e., the right boundary of the hole does not move appreciably.

In the first attempt at a run for $CRD = 0.1$, the automatic program being used at the time was unable to negotiate the sharp turn at the top of the hole. After some modification in the program, the run was tried again, and the plot of Fig. 13 resulted. This curve for $CRD = 0.1$ was felt to be a reasonable approximation to the desired curve. Although the hole is a little larger and the right-hand boundary is a little further to the left, a bearing design based on this approximate curve would at least be conservative, and thus it was decided to use $CRD = 0.1$ in obtaining stability plots for other values of W' .

As with Figs. 11 and 12, Fig. 13 was based on ten time steps per cycle. At the same time the run for Fig. 13 was made, a partial run was also made using identical data except with twenty time steps per cycle. The difference in the plots taken from these two runs was negligible; thus, it was decided that ten time steps per cycle was sufficiently accurate. Although the decisions made in this and the preceding paragraph were initially based on a limited amount of work, comparison of later

Fig. 13.--Stability plot for $W'=0.1$, $CRD=0.1$,
superimposed over the plot of Fig. 7.



results with those of Ref. [1] confirmed the validity of using $CRD = 0.1$ and ten time steps per cycle.

Other Values of W'

Because excessive computer time would have been required to obtain a full set of curves by the method used to establish Fig. 7, and since Fig. 13, based on short-cut methods, is a reasonable approximation to the more-accurate plot, it was decided to base the stability curves for other values of W' on $CRD = 0.1$, $DIST = 0.025$, ten time steps per cycle, and fifty cycles for stability. Although no complete curves were available as a means of checking these approximate curves, the results of Ref. [1] were used to verify them in all except the hole regions. Stability plots for various values of W' , from both this approximate method and the results of [1], are presented in Figures 14 through 16. Some of these curves are plotted individually, rather than in a family as before, because otherwise the overlapping of their hole regions would cause confusion. In most cases the agreement between the two sets of curves is good. For the higher values of W' , there is some discrepancy, especially for $W' = 0.5$, but even here a bearing design based on the new data would be conservative.

It is especially interesting to compare the new curves with those of [1] for the particular values of W' equal to 0.4, 0.3, 0.2, and 0.15. Remembering that the

Fig. 14.--Stability plots for $W'=0.6$, 0.5 , 0.4 , and 0.3 ; based on $CRD=0.1$; superimposed over the corresponding curves from Fig. 4.

(Broken curves are from Fig. 4.)

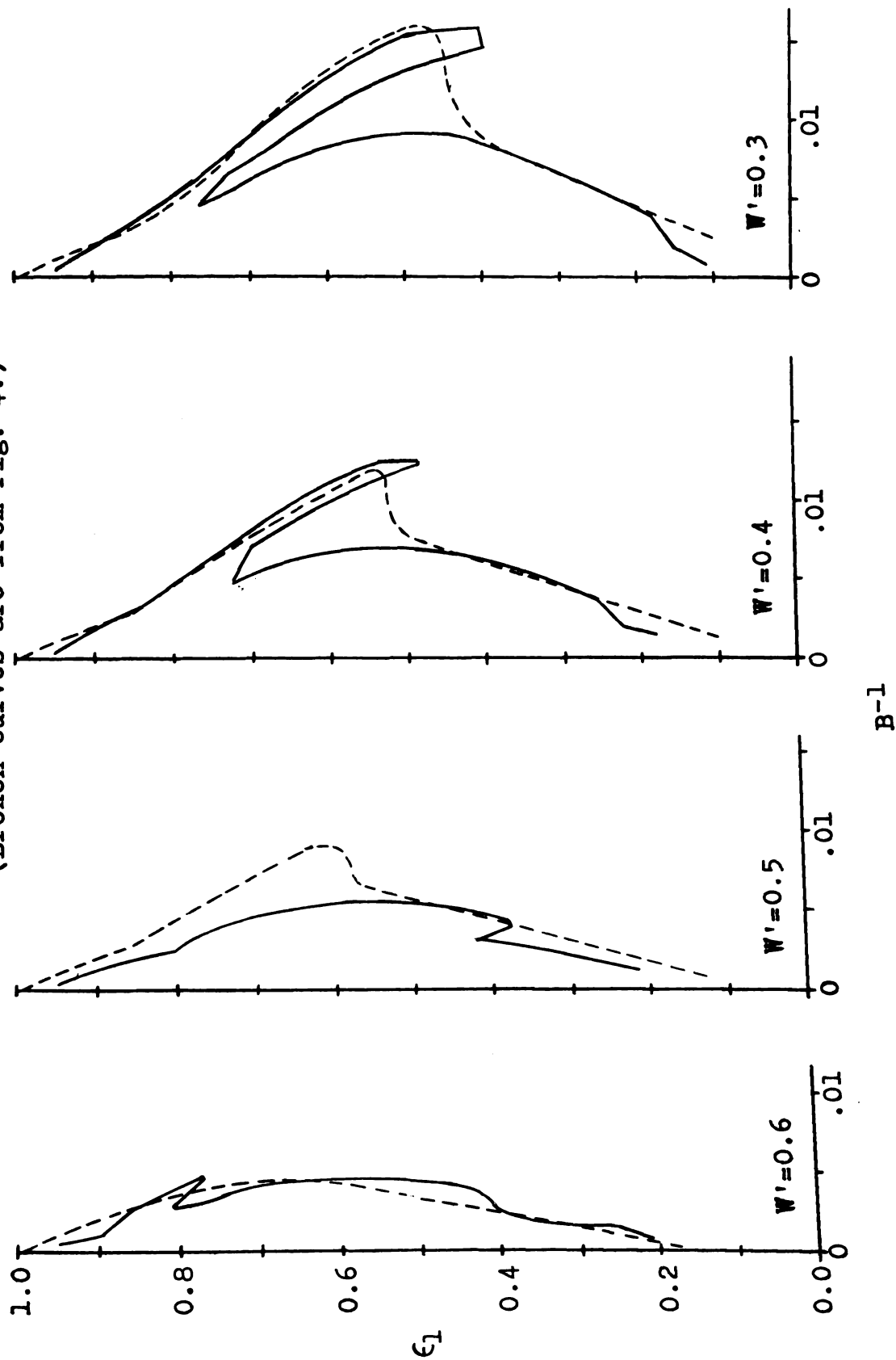


Fig. 15.--Stability plots for $W'=0.2$ and 0.15 , based on $CRD=0.1$,
superimposed over the corresponding curves from Fig. 4.
(Broken curves are from Fig. 4.)

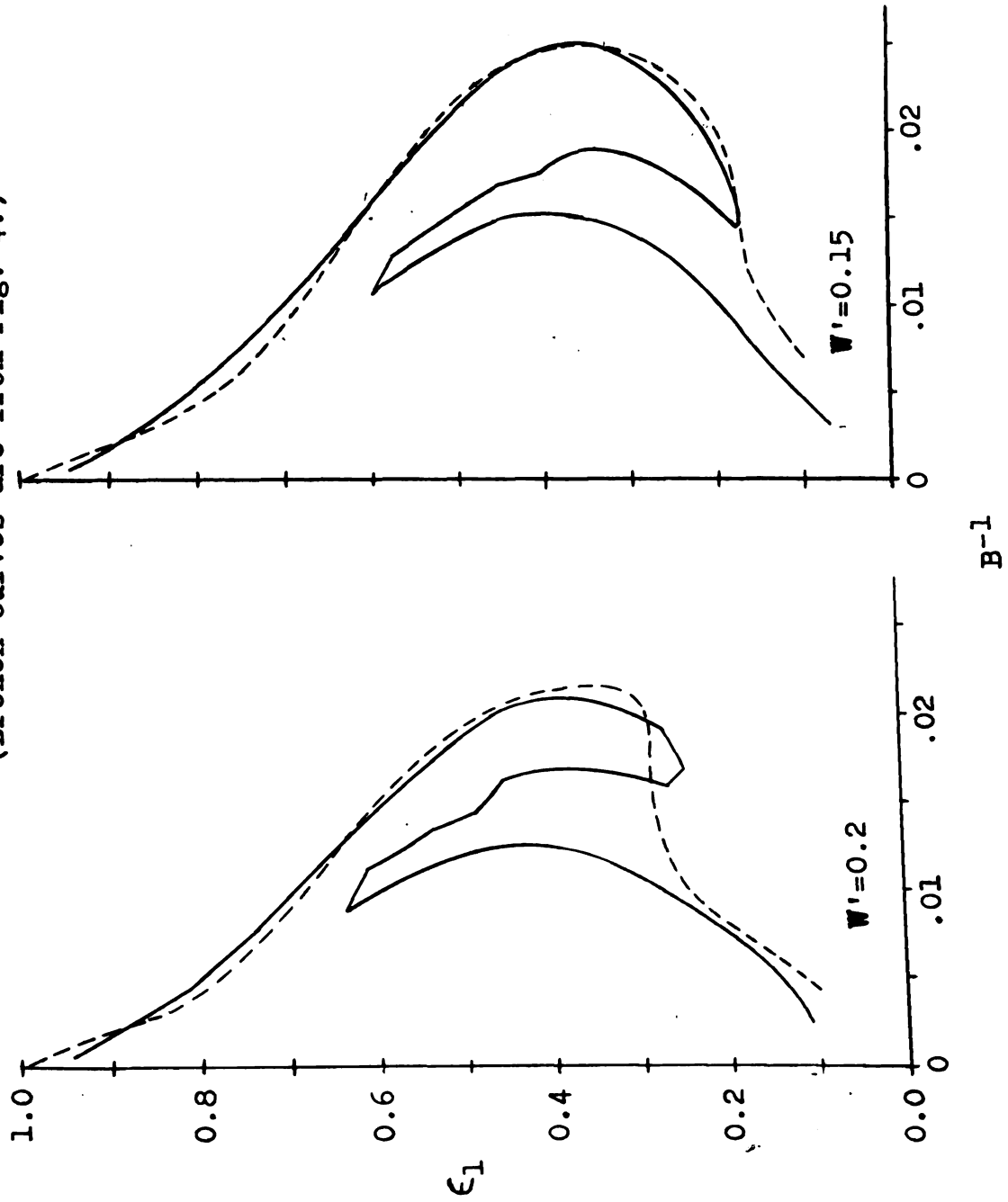
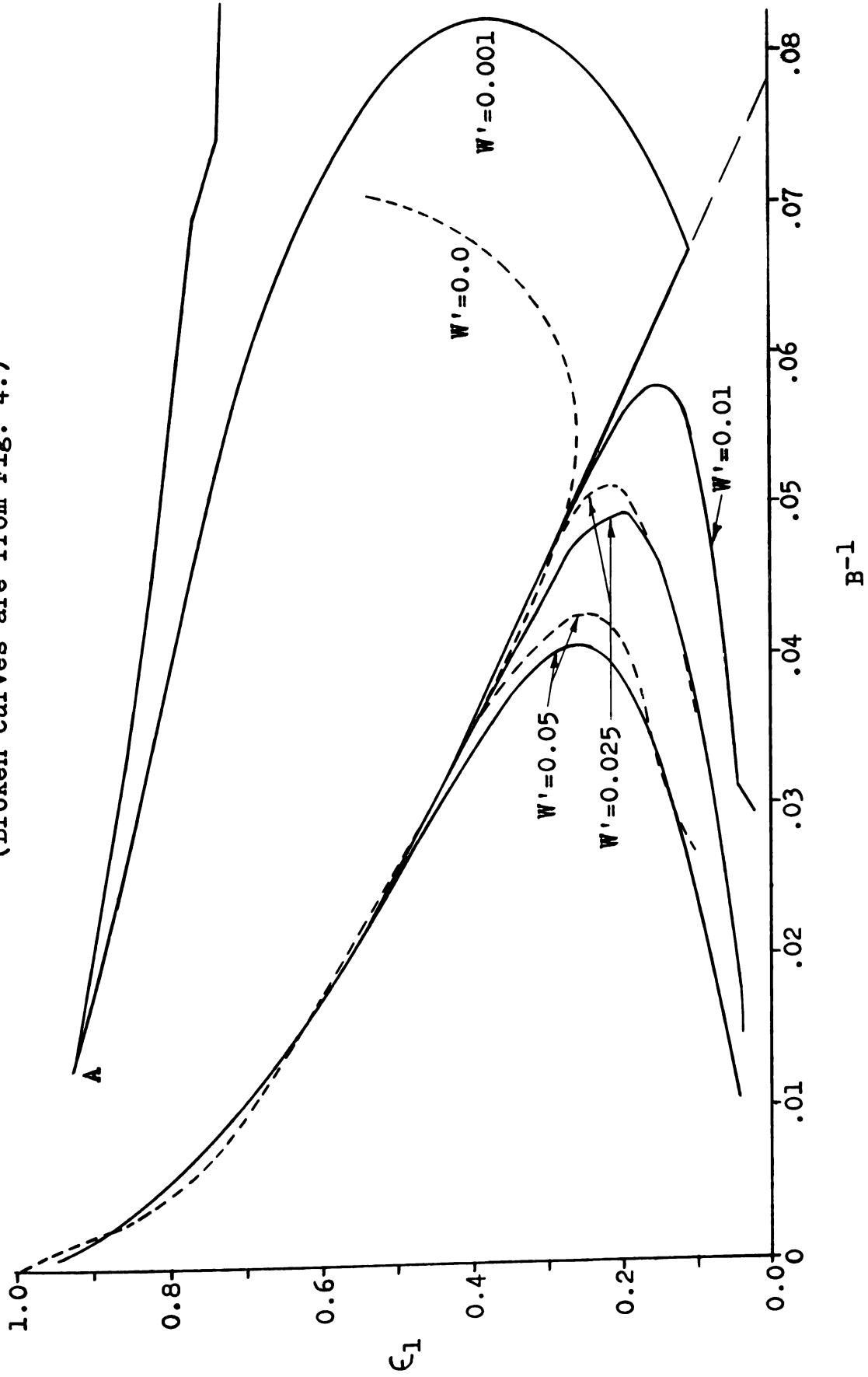


Fig. 16.--Stability plots for $W'=0.05$, 0.025 , 0.01 , and 0.001 ; based on $CRD=0.1$; superimposed over curves from Fig. 4 for $W'=0.05$, 0.025 , and 0.0 .
(Broken curves are from Fig. 4.)



method used in [1] searched only on a straight-line path from right to left, it should be clear how the holes were jumped over. The results of the two methods for these values of W' agree quite well in all regions except the holes.

No holes were located for values of W' less than 0.1. Curves for $W' = 0.05$ and 0.025 are given in Fig. 16; the agreement here between the two methods is quite satisfactory. Note that the new results are plotted to lower values of ϵ_1 ; these are the lowest values of ϵ_1 capable of supporting the given W' in a stable manner. For lower values of ϵ_1 , the corresponding increase in ϵ_2 which would be necessary to keep supporting the load would cause the sum of ϵ_1 and ϵ_2 to exceed unity--thus instability.

An especially interesting, although not so practical, case stems from the curve proposed in [1] for $W' = 0.0$ (See Fig. 4). Since compatible values of ϵ_1 and ϵ_2 were not available for $W' = 0.0$, an attempt was made to approach this curve by testing cases of small, but not zero, W' . Fig. 16 shows the curves for $W' = 0.01$ and 0.001 along with the one given in Fig. 4 for $W' = 0.0$. The curve for $W' = 0.01$ follows the trend of those given for larger values of W' , with its stable region extending even further to the right than in the case of $W' = 0.025$. The curve for $W' = 0.001$ does loop back as predicted in

[1], although the loop occurs at larger values of B^{-1} than predicted. The loop continues back to the point indicated by "A", where the curve takes a very sharp change in direction and extends out to the right as shown (It was necessary to modify the searching logic again before the turn at point A could be negotiated.) Since the program was written to terminate if any values of B^{-1} larger than 0.1 were encountered, the plot was not obtained past that point. However, the trend of the curve at the point of termination was still gradually inclined downward to the right as shown. It was decided that the case of $W' = 0.001$ was not of sufficient practical interest to warrant a further investigation of the curve.

It is of interest to mention the savings of computer time realized by the use of the short-cut method. For thirteen different cases, including those plotted in Figs. 14 through 16, the total computer time was less than ten minutes--a considerable improvement over the forty-five minutes required for the single plot of Fig. 7.

STABILITY OF THE FINITE JOURNAL BEARING IN ONE DEGREE OF FREEDOM

While the stability plots presented thus far in this paper have given much information of interest concerning the general nature of stable and unstable regions of operation for various combinations of system parameters, the analysis, as mentioned before, was based on a mass-content rule which is restricted to journal bearings of infinite length. Use of this mass-content rule was justified because, first, at one time it was the best available, and, secondly, stability plots based on it required much less computer time than those based on the less-restrictive rule. However, because typical length-to-radius ratios currently of interest are in the neighborhood from 1.0 to 2.0, the development of some stability criteria based on a mass-content rule for finite bearings was felt to be in order.

Mass-Content Rule for Finite Bearings

The more-general mass-content rule was developed by Beck and Strodtman [16]. As with the Elrod mass-content rule (Eq. 17), the derivation of this one begins with the Reynolds equation. Using Eq. (16) to eliminate P from Eq. (4) gives

$$\frac{\partial}{\partial Z} \left[\Psi H \frac{\partial \Psi}{\partial Z} - \Psi^2 \frac{\partial H}{\partial Z} \right] + \frac{\partial}{\partial \theta} \left[\Psi H \frac{\partial \Psi}{\partial \theta} - \Psi^2 \frac{\partial H}{\partial \theta} \right] = \sigma \frac{\partial \Psi}{\partial t} \quad (29)$$

Assuming Ψ to be periodic in time at every point after steady-state is reached (which seems reasonable since the squeeze input is periodic), averaging this equation over a number of cycles in time gives

$$\overline{\frac{\partial}{\partial Z} \left[\Psi H \frac{\partial \Psi}{\partial Z} - \Psi^2 \frac{\partial H}{\partial Z} \right]} + \overline{\frac{\partial}{\partial \theta} \left[\Psi H \frac{\partial \Psi}{\partial \theta} - \Psi^2 \frac{\partial H}{\partial \theta} \right]} = 0 \quad (30)$$

where the bars above terms denote time-averages. For large squeeze numbers, Ψ is independent of time--see Eqs. (14), (15), and (16); thus (30) can be rewritten

$$\frac{\partial}{\partial Z} \left[\bar{H} \Psi \frac{\partial \Psi}{\partial Z} - \Psi^2 \frac{\partial \bar{H}}{\partial Z} \right] + \frac{\partial}{\partial \theta} \left[\bar{H} \Psi \frac{\partial \Psi}{\partial \theta} - \Psi^2 \frac{\partial \bar{H}}{\partial \theta} \right] = 0 \quad (31)$$

An expression for H is given by Equation (12). At the position of equilibrium, where the journal is assumed to be held until the bearing is pumped up to satisfy the mass-content rule, $Y = \epsilon_2$. Then for purposes of deriving the mass-content rule, (12) can be written

$$H = 1 - \epsilon_2 \cos \theta - \epsilon_1 \sin(t) \quad (32)$$

From this,

$$\bar{H} = 1 - \epsilon_2 \cos \theta \quad (33)$$

$$\frac{\partial H}{\partial Z} = 0 = \frac{\partial \bar{H}}{\partial Z} \quad (34)$$

and

$$\frac{\partial H}{\partial \theta} = \epsilon_2 \sin \theta = \frac{\partial \bar{H}}{\partial \theta} \quad (35)$$

Putting (33), (34), and (35) into (31), and defining

$$T = \Psi^2, \quad (36)$$

Eq. (31) can be written

$$\frac{\partial}{\partial Z} \left[\frac{1 - \epsilon_2 \cos \theta}{2} \frac{\partial T}{\partial Z} \right] + \frac{\partial}{\partial \theta} \left[\frac{1 - \epsilon_2 \cos \theta}{2} \frac{\partial T}{\partial \theta} - T \epsilon_2 \sin \theta \right] = 0 \quad (37)$$

In the development of Elrod's mass-content rule, T was assumed to be independent of Z , except possibly in the very narrow end regions at infinity, and so the first term of Eq. (37) was omitted, and the explicit expression for Ψ given by Eq. (17) resulted. Since the present analysis is for finite-length bearings, such a simplification cannot be made; it is necessary to solve Eq. (37) as it stands. Unfortunately, no neat analytical expression for T could be derived which would satisfy this equation. Therefore, Strodtman developed a computer program which would solve the equation using finite-difference techniques.

The particular technique used by Strodtman in the solution of (37) is the Peaceman-Rachford alternating-direction method [17]. To use this method, the film is considered to be broken up into an M by N matrix, with M nodes in the Z direction from one end to the center, and N nodes in the θ direction from 0 to π ; advantage is taken of symmetry in both the Z and θ directions. An initial array of T values is specified, and then iterations are made, alternating in the Z and θ directions, until both Eq. (37) and the following boundary conditions are satisfied:

$$T(\theta, 0) = (1 - \epsilon_2 \cos \theta)^2 + \frac{3}{2} \epsilon_1^2 \quad (38)$$

and

$$\frac{\partial T}{\partial \theta}(0, Z) = \frac{\partial T}{\partial \theta}(\pi, Z) = \frac{\partial T}{\partial Z}(\theta, \frac{L}{2R}) = 0 \quad (39)$$

Conditions (39) are obvious from symmetry considerations, while (38) is a special case of a more-general boundary condition developed in Ref. [16].

When Strodtman developed the computer program **SHORTJ** to solve Eq. (37), it was with the intention of constructing load curves for finite bearings of various length-to radius ratios, i.e., curves of W' versus ϵ_2 for various constant ϵ_1 as shown in Fig. 3 for infinite journals. Thus, convergence of his iteration procedure was based on convergence of W' calculated from

$$W' = -2\frac{R}{L} \int_0^\pi \int_0^{\frac{L}{2R}} \frac{\sqrt{T} \cos \theta \, dZ d\theta}{\sqrt{(1 - \epsilon_2 \cos \theta)^2 - \epsilon_1}} \quad (40)$$

Because no analytical expression for T as a function of Z and θ was available, it was necessary to perform the double integration in (40) numerically; Simpson's rule was used.

Two families of load-support curves (for length-to-radius ratios of 1 and 2) are given in Figures 17 and 18. It is interesting that the load support produced by a finite bearing is higher than that for an infinite bearing (Compare with Fig. 3.)

Fig. 17.--Load-support curves for bearings with a length-to-radius ratio of unity.

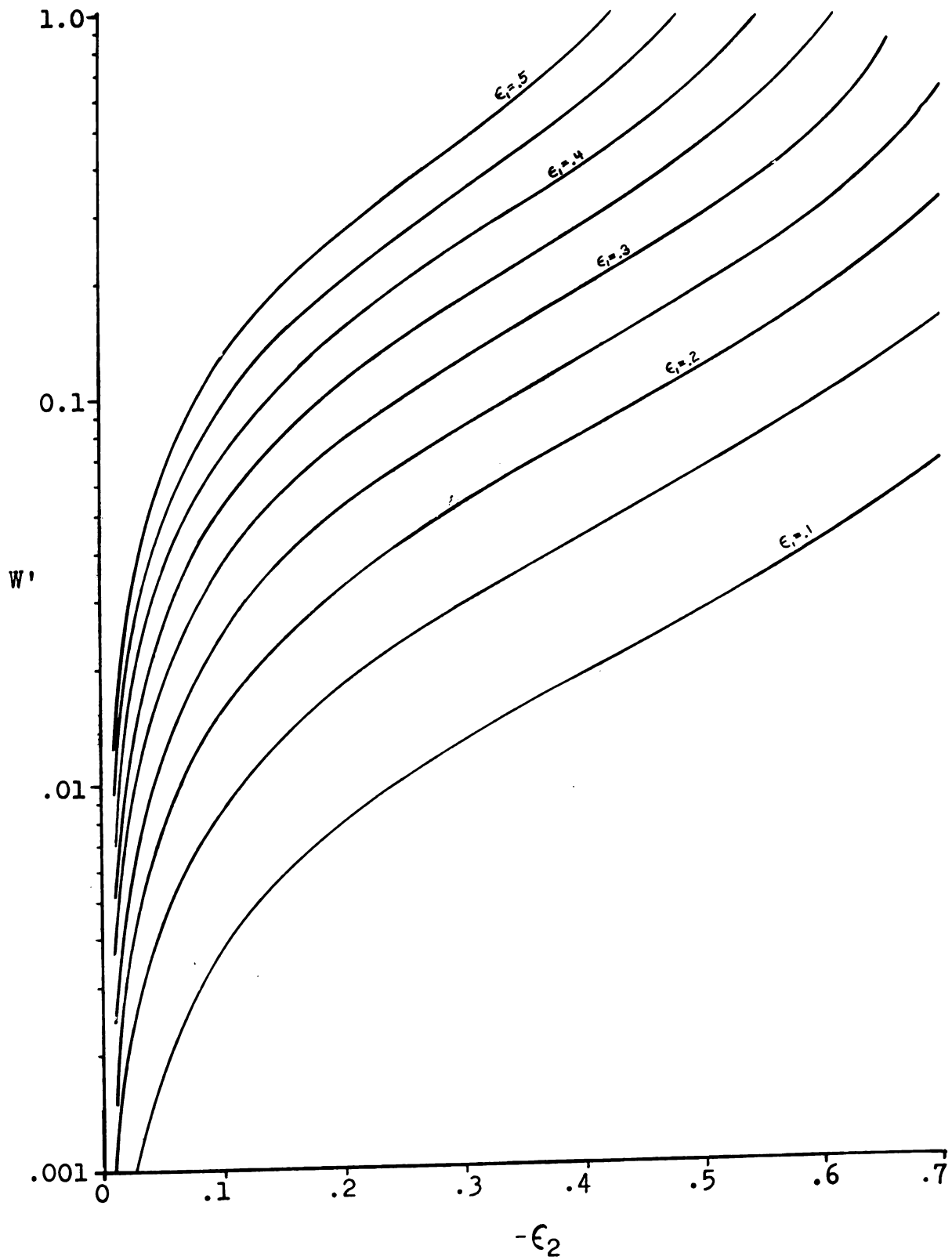
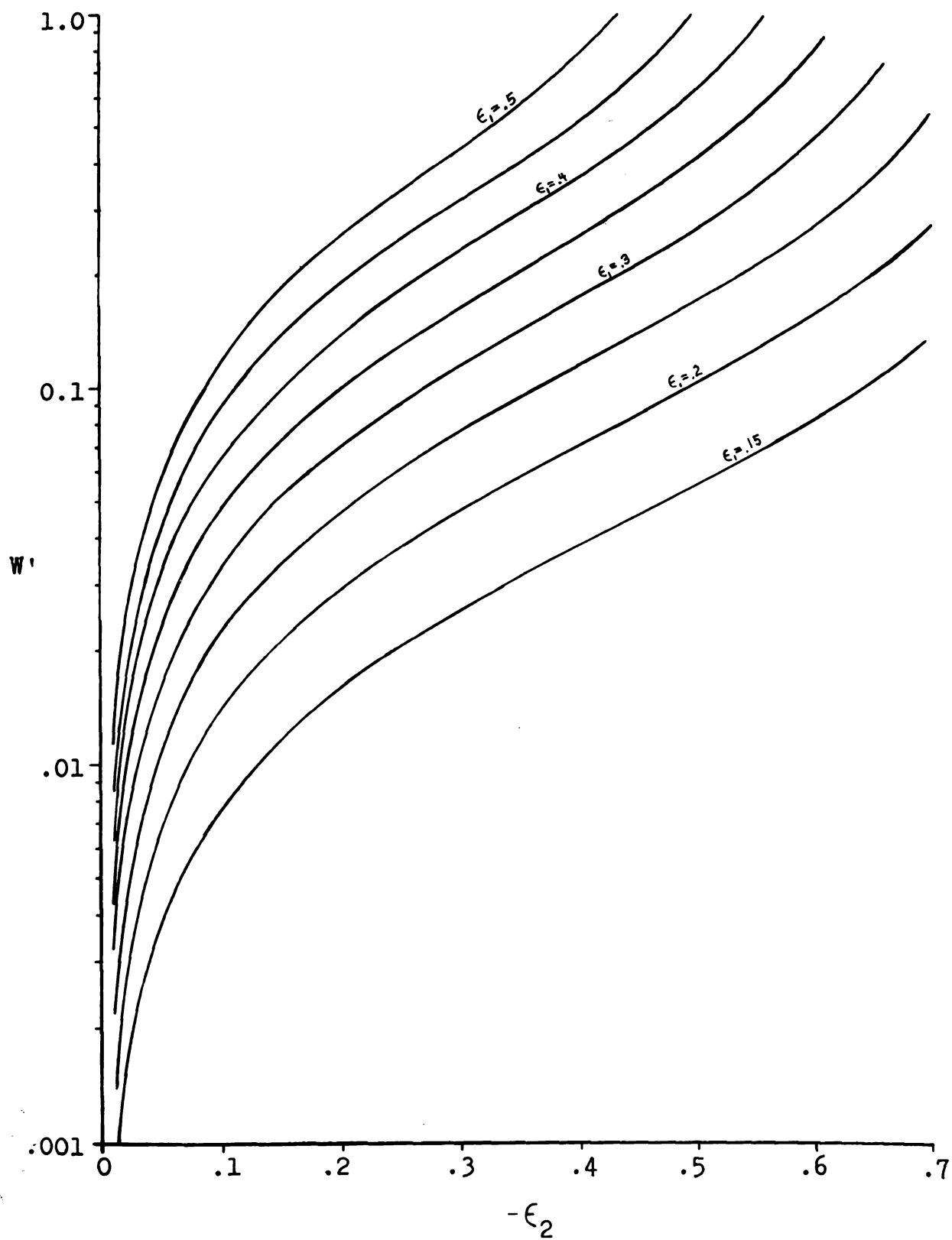


Fig. 18.--Load-support curves for bearings with
a length-to-radius ratio of 2.0.



Equation of Motion for Finite Bearings

Equation (10) is a valid equation of motion for journal bearings of finite length which are constrained to motion only in the Y coordinate; it is repeated here for convenience.

$$\frac{d^2Y}{dt^2} = - \frac{1}{B} \left[\frac{4R}{L} \int_0^\pi \int_0^{\frac{L}{2R}} P(\cos\theta) dz d\theta + 2W' \right] \quad (10)$$

In general, P in the above integral will be a function of both Z and θ . It can be expressed in terms of Ψ and H (See Eq. 20) as

$$P = \frac{\Psi}{H} \quad (41)$$

An expression for H is given in Eq. (12), and, since SHORTJ works with T instead of Ψ , it is better to replace Ψ with \sqrt{T} ; thus (41) becomes

$$P = \frac{\sqrt{T}}{1 - Y\cos\theta - \epsilon_1\sin(t)} \quad (42)$$

Putting (42) into (10) gives the equation of motion which must be solved for bearings of finite length:

$$\frac{d^2Y}{dt^2} = - \frac{1}{B} \left[\frac{4R}{L} \int_0^\pi \int_0^{\frac{L}{2R}} \frac{\sqrt{T} \cos\theta}{1 - Y\cos\theta - \epsilon_1\sin(t)} dz d\theta + 2W' \right] \quad (43)$$

Since no analytical expression for T as a function of Z and θ is available, the double integral above was evaluated with Simpson's rule in two dimensions, using the same number of nodes in the Z and θ directions as were used in SHORTJ so that there would be a value of T avail-

able for each node. Once compatible values of ϵ_1 , ϵ_2 , W' , and the corresponding T array are obtained from SHORTJ, Eq. (43) is solved in the same manner as was (20).

Searching in Other Coordinates

In the case of the infinite journal, the automatic searching procedure was carried out in the ϵ_1 versus B^{-1} plane for curves of constant W' . As the program "felt" its way along the curve, the value of ϵ_1 changed, and the corresponding values of ϵ_2 , which would be compatible with each new ϵ_1 and the value of W' for the curve, were needed. These values of ϵ_2 were found by interpolating in a table of values of ϵ_1 and ϵ_2 ; this table was read into the program as part of the data for each new value of W' . Because no more than forty storage locations were required to accomodate the complete table, this method proved to be quite satisfactory.

In the present case of the finite bearing, compatible values of ϵ_1 and ϵ_2 for a given W' could be taken from curves like those of Figs. 17 and 18 for the appropriate length-to-radius ratio, and the values of ϵ_2 needed in the program could again be found by interpolation. However, the problem which arises in this finite-journal case is not with ϵ_2 , but with the T in Eq. (43). In the infinite-journal case, once ϵ_1 and ϵ_2 were known, the integrand of Eq. (20) could be calculated, because it was an analytical function of ϵ_1 and ϵ_2 . In the present

case, T cannot be expressed analytically in terms of ϵ_1 and ϵ_2 , but, at best, distinct numerical values of T at each node can be obtained from SHORTJ for each combination of ϵ_1 and ϵ_2 for a given W' . Then, if the intent is to conduct the search procedure in the ϵ_1 versus B^{-1} plane as before, the interpolation table must include not only compatible values of ϵ_1 and ϵ_2 , but also the corresponding T arrays. There are many disadvantages to this method. First, very-complete sets of data from SHORTJ would have to be run, and the resulting values of W' , ϵ_1 , ϵ_2 , and T arrays would have to be saved. Secondly, since W' is an output of SHORTJ, it cannot be specified in convenient round-number values; thus, if a constant- W' curve is to be run, values of ϵ_2 and T arrays for the chosen value of W' would have to be determined by interpolation in the complete sets of data mentioned above. Thirdly, even if sets of ϵ_1 , ϵ_2 , and T were available for a given W' , all of the values would have to be stored in the computer memory before the program could be executed; this would require much more input data than before, and it is doubtful that the capacity of the computer memory would be large enough to accept this data and the program simultaneously. Finally, if the program had been brought to the point of execution, the minimum-sized T array used (21 X 21) would have required 442 interpolations at each point tested, and this

would probably have required excessive computer time.

In order to circumvent many of the above problems, it was decided to conduct the search routine in terms of coordinates which could be prescribed independently of the results of SHORTJ, i.e., instead of plotting curves of constant W' , plot them for constant ϵ_1 or ϵ_2 . Then when a test point is located in the new coordinates, SHORTJ could be called as a subroutine to generate the corresponding W' and T arrays--no interpolations being necessary.

Numerous representations of stability were constructed graphically from the data of Figs. 13 through 16 in an attempt to determine which variables should be plotted on the ordinate and abscissa and which should be held constant in the new program. After comparing the various possibilities, it was decided that the search should take place in a plot of ϵ_2 versus B^{-1} with ϵ_1 held constant. Such curves, constructed from the previously-given data for infinite bearings, are shown in Fig. 19 for ϵ_1 values of 0.3, 0.5, and 0.8. The first step in constructing these curves was to tabulate compatible values of W' versus B^{-1} for each ϵ_1 of interest; these values were obtained from Figs. 13 through 16. Then compatible values of ϵ_2 for each (ϵ_1, W') combination were obtained from Fig. 3, and these values of ϵ_2 were plotted versus B^{-1} on curves of constant ϵ_1 in

Fig. 19.--Stability plots of ϵ_2 versus B^{-1} for $\epsilon_1=0.8, 0.5$, and 0.3 ; constructed from the data of Figs. 13-16.

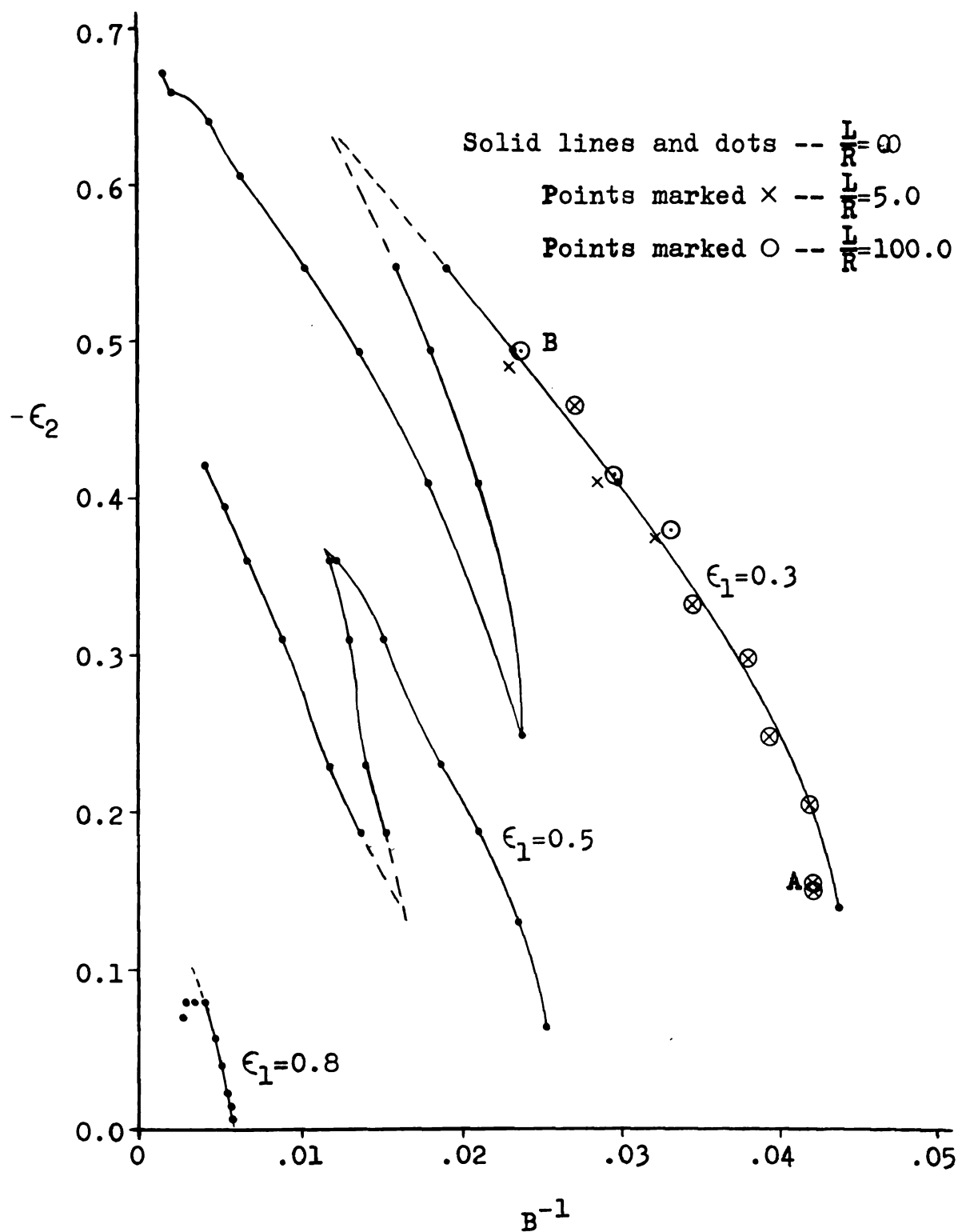


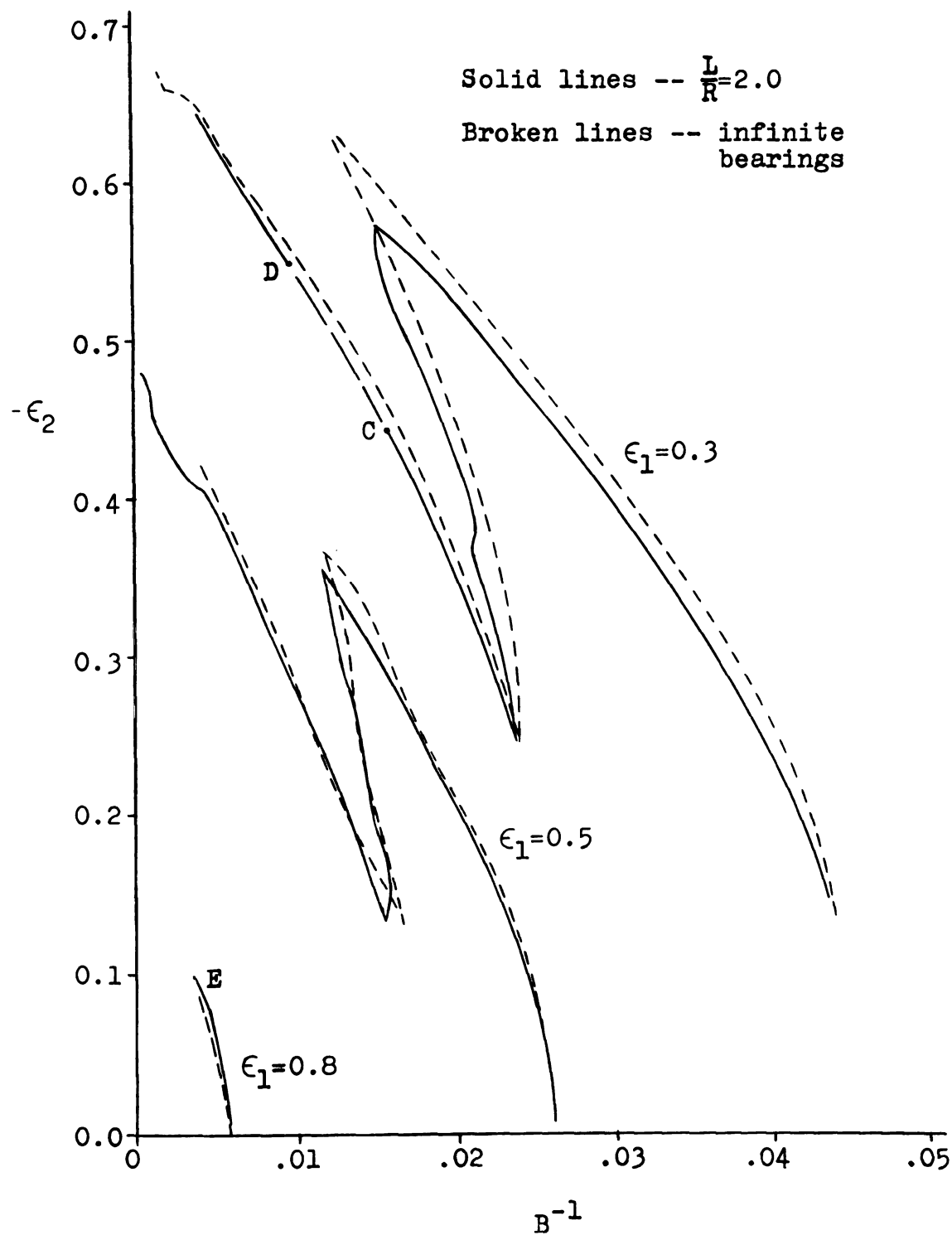
Fig. 19.

Plots of ϵ_2 versus B^{-1} Independent of L/R

The first successful stability program for finite bearings was an attempt to locate the right-hand boundary of the plot for $\epsilon_1 = 0.3$ in the ϵ_2 versus B^{-1} plane. Data was read in for length-to-radius ratios of 100, 10, 5, and 2, and it was anticipated that the resulting stability curve for a ratio of 100 would be closest to the curve for the infinite ratio given in Fig. 19 for $\epsilon_1 = 0.3$, with the other curves falling further from this one as the value of L/R decreased. However, as closely as could be determined from the relatively coarse data being used at the time ($DIST = 0.1$), the curves for all values of L/R appeared to lie right on the curve for the infinite bearing--points for L/R values of 5 and 100 are plotted on Fig. 19. As these results were only obtained in the region between points A and B of Fig. 19, another more-complete run was made for $L/R = 2$.

For this more-complete run, $DIST$ was decreased to 0.02, CRD was 0.1, ten time steps per cycle were used, and fifty cycles were taken as the basis of stability. Three separate computer runs were required to establish the 128 points from which the two sections of curve shown in Fig. 20 were plotted. The gap between points C and D could have been filled in, but, since the rest of the

Fig. 20.--Stability plots of ϵ_2 versus B^{-1} for $\epsilon_1=0.8, 0.5, \text{ and } 0.3$; $\frac{L}{R} = 2.0$; superimposed over the corresponding curves for infinite bearings.



curve followed the one for the infinite journal so well, it was decided that this section need not be tested.

After the unexpected similarity between the curves of Fig. 20 for $\epsilon_1 = 0.3$, data was run for ϵ_1 values of 0.5 and 0.8; the results of these runs are also shown in Fig. 20. Although the program for $\epsilon_1 = 0.8$ was terminated at point E, due to a limitation of one of the subroutines, it was decided that the curves presented thus far were sufficient evidence to conclude that stability plots in the ϵ_2 versus B^{-1} plane for curves of constant ϵ_1 are essentially independent of the length-to-radius ratio.

Constructing Stability Plots for Finite Journals

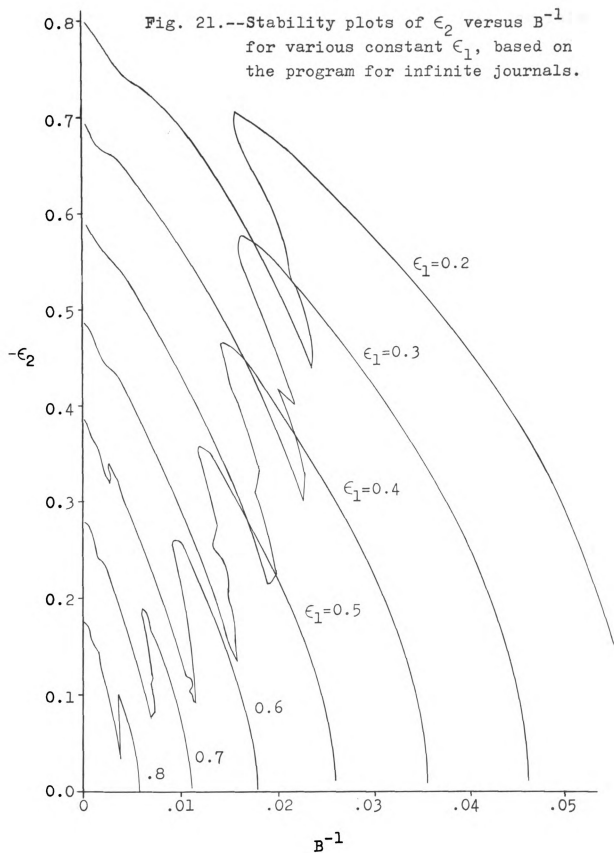
Although stability plots in the ϵ_2 versus B^{-1} plane were found to be very nearly the same for any length-to-radius ratio, the same conclusion cannot be reached for stability plots in the ϵ_1 versus B^{-1} plane at constant W' (as were used previously). These latter plots are more meaningful representations of stability because W' is a more meaningful system parameter than is ϵ_2 ; i.e., while the values of ϵ_1 , W' , and B^{-1} can be controlled, at least to some extent, ϵ_2 is the resulting equilibrium displacement, and its value depends on the values of the other three parameters; ϵ_2 can be thought of as a dependent quantity, while the other three are independent.

Even though the plots of ϵ_2 versus B^{-1} at constant

ϵ_1 are not particularly useful representations of stability, the fact that they are essentially the same for all length-to-radius ratios suggests a technique for the construction of plots of ϵ_1 versus B^{-1} at constant W' for finite bearings of a given L/R . This technique is based on the curves of ϵ_2 versus B^{-1} at constant ϵ_1 (independent of L/R) and on the load-support curves (e.g., Figs. 17 and 18) for the particular length-to-radius ratio of interest. The method is essentially the reverse of that used in the construction of Fig. 19.

Because the procedure for any value of L/R began with curves of ϵ_2 versus B^{-1} at constant ϵ_1 , a complete family of these curves was desired. These curves could have been obtained by using the computer program for finite bearings, but, since the resulting curves from the program for infinite journals have been shown to be essentially the same, this latter program was used, with a considerable savings of computer time. Such curves were obtained for values of ϵ_1 from 0.1 through 0.8 in increments of 0.05; several of them are plotted in Figure 21.

In the computer program used, the stable and the unstable boundary points were plotted individually, but on the same set of axes. The curves of Fig. 21 were then traced directly from the plotter output by drawing between the curves of stable and unstable points. Thus,



the occasional irregular trends of these curves are felt to be correct, and in some locations, especially near the tops of these curves, it seems quite possible that other hole regions may exist. While such regions could be investigated more thoroughly by using smaller distances between test points, more cycles for stability, etc., it is felt that the present set of curves are sufficiently accurate for this investigation.

Starting with the curves of Fig. 21, it is desired to construct stability plots in the (ϵ_1, B^{-1}) plane for finite bearings. Such stability curves depend in general on the value of length-to-radius ratio of interest. In any case, the method of construction is the same, and it will be outlined here for the particular ratio of unity. For a given length-to-radius ratio, the values of ϵ_1 and ϵ_2 at a given point of Fig. 21 define a specific value of W' . For the present case, with L/R of unity, these values of W' were obtained from the load curves of Fig. 17. Thus, curves of W' versus B^{-1} at constant ϵ_1 were constructed. This was done for values of ϵ_1 between 0.1 and 0.5 at intervals of 0.05. If the (ϵ_1, B^{-1}) pairs for a given W' are taken from these curves, a stability plot in the ϵ_1 versus B^{-1} plane at that constant W' can be plotted. The results of such construction are presented in Figs. 22 and 23 for various values of W' . The broken lines in these figures duplicate the previously-

Fig. 22.--Partial stability plots of ζ_1 versus B^{-1} for $\frac{L}{R} = 1.0$, superimposed over the corresponding plots for an infinite journal.

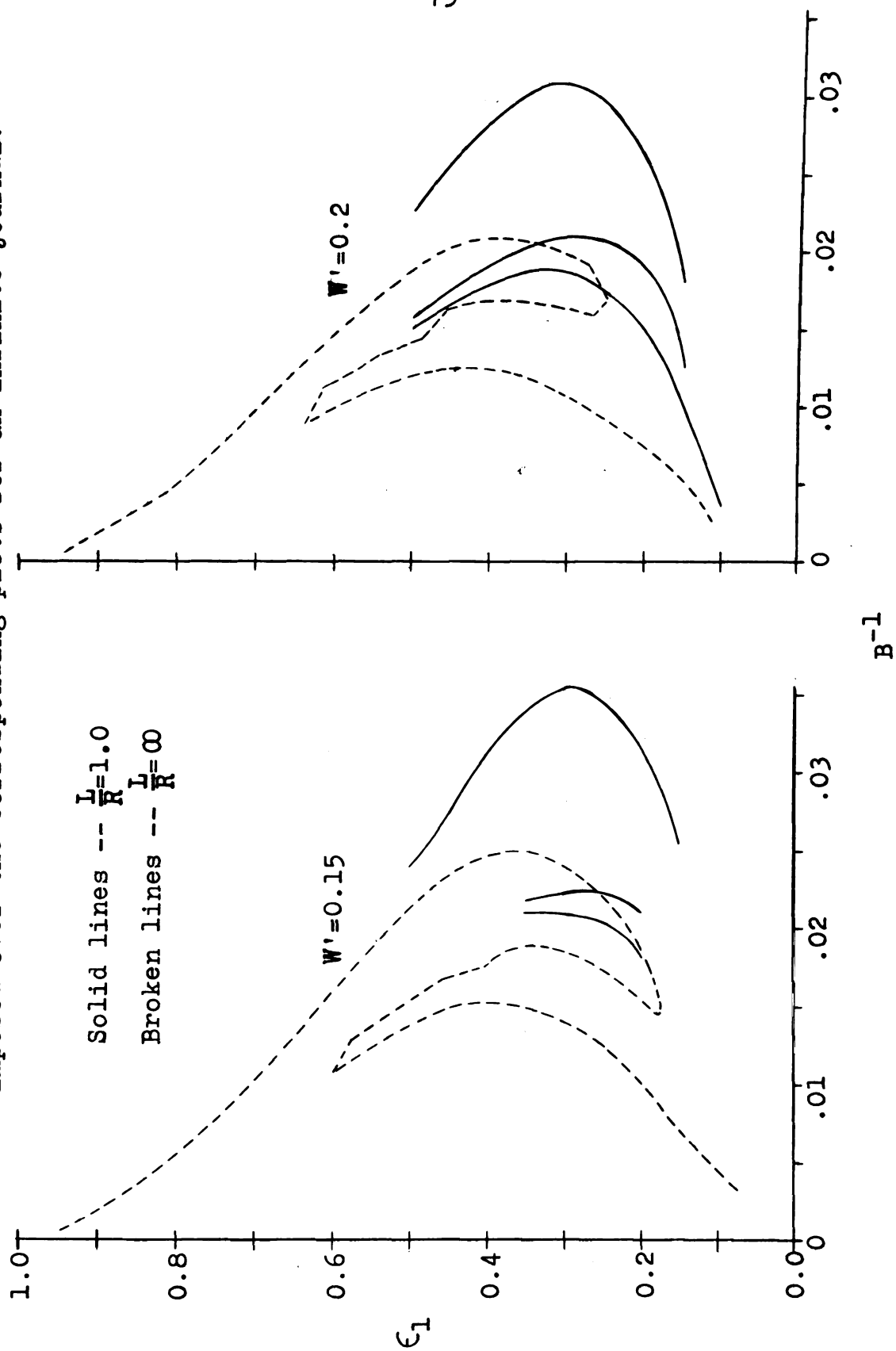
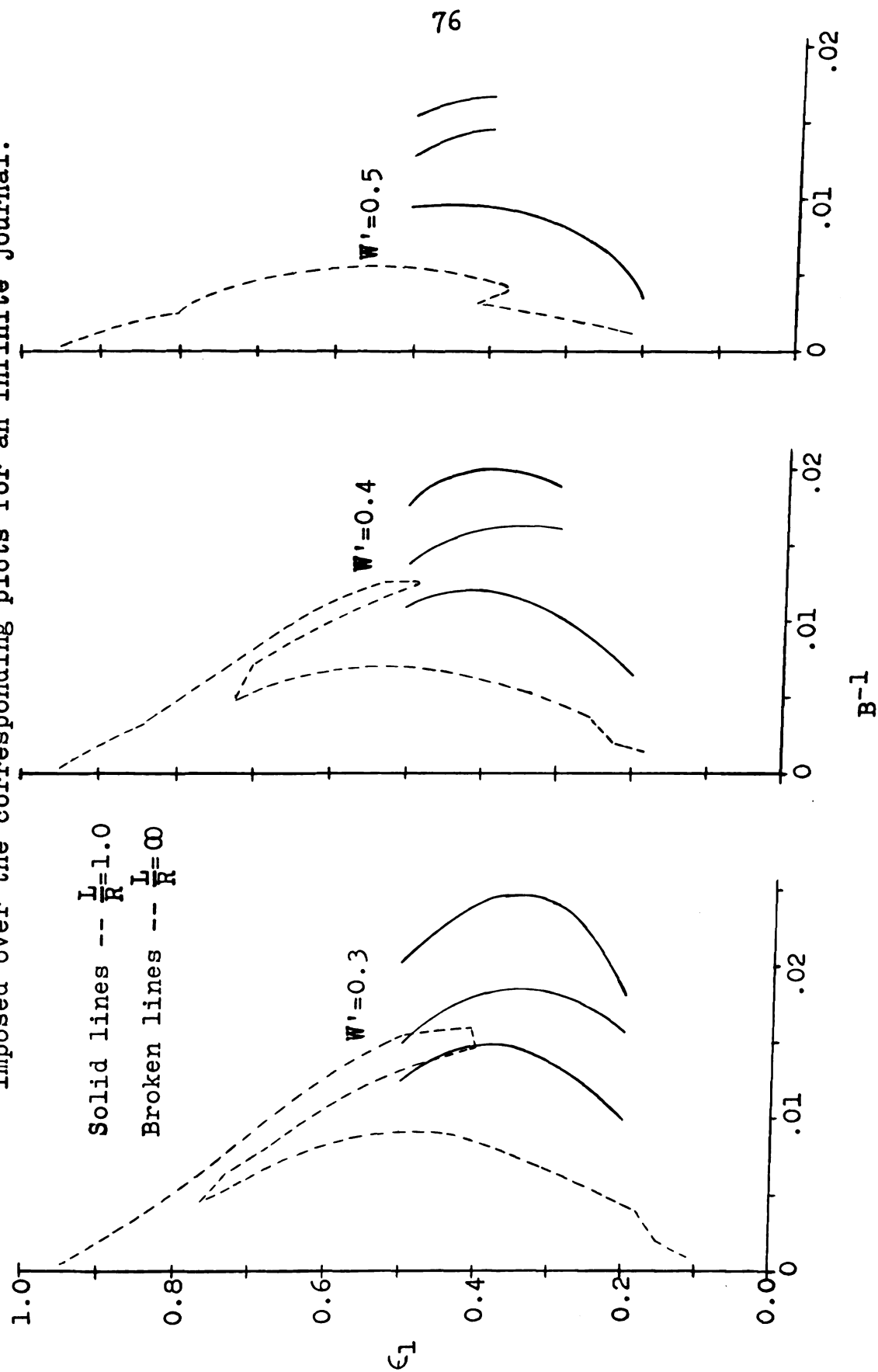


Fig. 23.--Partial stability plots of ζ_1 versus B^{-1} for $\frac{L}{R} = 1.0$, superimposed over the corresponding plots for an infinite journal.



plotted results from the case of the infinite journal (Figs. 14 and 15). The curves for the finite bearing are incomplete because the load-support curves of Fig. 17 were only given for ϵ_1 between 0.1 and 0.5. While a more-complete set of these curves could have been obtained, the portions of plots already shown in Figs. 22 and 23 are sufficiently complete to compare the stability regions of the finite journal with those of the infinite journal. It appears that the two sets of curves would merge at $\epsilon_1 = 0.0$ and at $\epsilon_1 = 1.0$, and a more-complete construction would probably only verify this.

Comparison of the Finite and Infinite Bearings

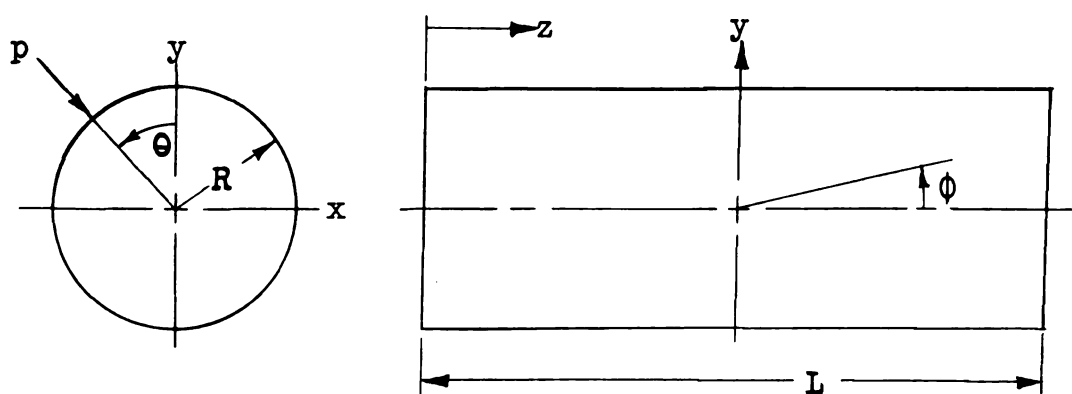
The curves shown in Figs. 22 and 23 indicate that the stability characteristics of finite journal bearings with L/R of unity are better than those for infinite journal bearings. Because the method of construction of such stability curves depends directly on the family of load-support curves for the L/R of interest, and because it is shown in Ref. [16] that load-support increases with decreasing L/R , it seems safe to assume that stability curves for all finite journal bearings will fall to the right of those for infinite journal bearings when plotted in the (ϵ_1, B^{-1}) plane. Thus, the infinite journal bearing will have the least desirable stability characteristics of any, and any design based on the stability curves of an infinite bearing should be conservative.

STABILITY OF THE FINITE JOURNAL BEARING IN MORE-THAN-ONE DEGREE OF FREEDOM

Up to this point, the analysis has been restricted to journals constrained to move only in a single translational coordinate normal to their axes and in the direction of the applied load. The purpose of the present section is to investigate stability characteristics of finite journal bearings in more-than-one degree of freedom. A preliminary small-parameter analysis showed that, for the four coordinates listed on page 8, the equation of motion for the second translational coordinate is quite like the one already studied, and that the equations of motion in the two angular coordinates are quite similar to each other. It was decided that if motion in only one additional coordinate were going to be allowed, it should be one of the angular coordinates, since motion in the other translational coordinate would probably yield essentially the same stability plots as before. In order to confine all motion of the journal to a single plane, the coordinate described by point (4) on page 8 was chosen for the second degree of freedom.

The two coordinates used in the two-degree-of-freedom case are defined in Fig. 24. The y-coordinate speci-

Fig. 24.--Configuration of the two-degree-of-freedom system.



fies the vertical location of the center of gravity of the journal as before, and ϕ indicates the angular orientation of the journal about its center of gravity.

The distance z is measured from the left end of the journal as shown, to be consistent with previous work, and the angle θ is also defined as before.

Equation (7) is still a valid dimensionless equation of motion in the Y coordinate, but it can no longer be reduced to the form of Eq. (10) because axial symmetry no longer exists in general. However, symmetry in θ is still present, so (7) can be written

$$\frac{d^2 Y}{dt^2} = - \frac{1}{B} \left[\frac{2R}{L} \int_0^\pi \int_0^{\frac{L}{R}} P(\cos\theta) dz d\theta + 2W' \right] \quad (44)$$

The equation of motion in the ϕ coordinate is derived by applying Newton's second law of motion in the form

$$\sum T_{c.g.} = \frac{J_{c.g.}}{g_0} \ddot{\phi} \quad (45)$$

where the subscripts $c.g.$ indicate that the law is being applied about the center of gravity of the journal. Because the center of gravity is chosen as the reference point, any torques produced by applied loads would cancel out, so only those produced by pressure forces need be considered. A procedure similar to that used in the derivation of Eq. (6) leads to the following equation of motion for the ϕ coordinate:

$$\frac{J}{g_0} \ddot{\Phi} = -R \int_0^{2\pi} \int_0^L p(z - \frac{L}{2}) (\cos \theta) dz d\theta \quad (46)$$

The moment of inertia J for a solid cylinder about a line through its center of gravity perpendicular to its axis can be expressed in terms of its length L , radius R , and mass m as

$$J = \frac{mR^2}{12} \left[3 + \left(\frac{L}{R} \right)^2 \right] \quad (47)$$

Using this expression for J along with the substitutions $p = p_a P$, $z = ZR$, $\ddot{\Phi} = \omega^2 \frac{d^2 \phi}{dt^2}$, and $\phi' = \frac{R}{h_0} \phi$, Eq. (46) can be written in normalized form as

$$\frac{d^2 \phi'}{dt^2} = - \frac{24}{B \left(\frac{L}{R} \right) \left[3 + \left(\frac{L}{R} \right)^2 \right]} \int_0^\pi \int_0^{\frac{L}{R}} P \left(Z - \frac{L}{2R} \right) (\cos \theta) dZ d\theta \quad (48)$$

It was noticed during the derivation of this equation that defining ϕ' as above eliminated the need for an additional dimensionless group.

The method of solution of Eqs. (44) and (48) is the same as that used previously, i.e., as prescribed by Eqs. (23), (25), (26), and (27). However, as before, this method cannot be applied until an expression for P is known. Since the analysis will still be restricted to bearings operating at high squeeze numbers, P can still be expressed in terms of H and T as

$$P = \frac{\sqrt{T}}{H} \quad (49)$$

However, the introduction of the second degree of freedom causes the expression for H to be somewhat different. The derivation of this new H will begin with its dimensional counterpart h , and reference to Fig. 24 should help verify the following expression:

$$h = h_0 - h_1 \sin(\omega\tau) - y \cos\theta - (z - \frac{L}{2}) \sin\phi \cos\theta \quad (50)$$

This is made dimensionless by using $h = h_0 H$, $h_1 = \epsilon_1 h_0$, $\omega\tau = t$, $y = h_0 Y$, $z = ZR$, $\sin\phi = \phi$, and $\phi' = \frac{R}{h_0} \phi$, yielding

$$H = 1 - \epsilon_1 \sin(t) - \left[Y + (Z - \frac{L}{2R}) \phi' \right] \cos\theta \quad (51)$$

The two-degree-of-freedom analysis can then be performed by solving Eqs. (44) and (48) simultaneously, using (51) as the expression for H .

Some Analytical Considerations

Before solving the above equations on the computer, some general statements can be made regarding the solutions. Such analysis is worthwhile to provide some insight into the character of the solutions, thus helping to detect possible errors in the computer program. Since stability regions for motion in Y alone have been quite thoroughly discussed, the observations to be made here will involve mainly the ϕ' coordinate, both how overall stability is affected by allowing motion in ϕ' and what stability regions can be expected if only ϕ' is allowed to change, i.e., Y fixed.

The first observation is that unless ϕ' (or $\frac{d\phi'}{dt}$) is given some initial value other than zero, no subsequent motion in ϕ' will occur. This statement is based on a consideration of the system configuration and on an examination of Eq. (48). Consider the bearing to be held at $Y = \epsilon_2$, $\phi' = 0$, and pumped up to satisfy the mass-content rule. The resultant pressure distribution must be symmetrical along the length of the bearing, i.e., $P(Z, \theta)$ must equal $P(\frac{L}{R} - Z, \theta)$. Now if the journal is displaced in the Y coordinate, but not in ϕ' , this symmetry in pressure should still exist. Referring to Eq. (48), a plot of the quantity $(Z - \frac{L}{2R})$ versus Z from zero to $\frac{L}{R}$ results in a straight line which goes from $-\frac{L}{2R}$ at the left end of the bearing through zero at the center to $+\frac{L}{2R}$ at the right end. Thus, in the integration of $P(Z - \frac{L}{2R})dZ$, the contributions from the left half of the bearing are just canceled by those from the right half, and (48) reduces to

$$\frac{d^2\phi'}{dt^2} = 0$$

This equation provides for no motion in ϕ' unless the initial value of ϕ' or $\frac{d\phi'}{dt}$ is other than zero, and these possibilities have been prohibited. With no motion in ϕ' , the symmetry in pressure distribution remains, the right side of (48) goes to zero for the next time step, and this cycle repeats for all subsequent time steps.

The next observation is that, for small ϵ_1 , ϵ_2 , Y ,

and ϕ' , the stability regions in the ϕ' coordinate are always at least as large as those in the Y coordinate. This conclusion is based on a small-parameter analysis; the development will first be applied to the equation in the Y coordinate. It is desired to find an expression for P which will make the integral in Eq. (44) integrable. Reference [16] gives the following general expression for T which is valid for finite bearings with small ϵ_2 :

$$T \approx 1 + \frac{3}{2}\epsilon_1^2 - 2\epsilon_2 \cos\theta \cdot \left\{ 1 + \frac{3}{2}\epsilon_1^2 \left[1 - \cosh(Z) + \sinh(Z) \tanh\left(\frac{L}{2R}\right) \right] \right\} \quad (52)$$

Putting (51) and (52) into (49) gives

$$P = \frac{\left[1 + \frac{3}{2}\epsilon_1^2 - 2\epsilon_2 \cos\theta \left\{ 1 + \frac{3}{2}\epsilon_1^2 [1-G] \right\} \right]^{\frac{1}{2}}}{D - \epsilon_1 \sin(t)} \quad (53)$$

where

$$G = \cosh(Z) - \sinh(Z) \tanh\left(\frac{L}{2R}\right) \quad (54)$$

and

$$D = 1 - \left[Y + \left(Z - \frac{L}{2R} \right) \phi' \right] \cos\theta \quad (55)$$

If P is considered as a function of ϵ_1 and ϵ_2 , it can be expanded in a Maclaurin series about $\epsilon_1=0$, $\epsilon_2=0$. The first ten terms of this series are given by

$$\begin{aligned} P \approx & \frac{1}{D} + \frac{\sin(t)}{D^2} \epsilon_1 - \frac{\cos\theta}{D} \epsilon_2 - \frac{\sin(t)\cos\theta}{D^2} \epsilon_1 \epsilon_2 \\ & - \frac{\cos^2\theta}{2D} \epsilon_2^2 + \left[\frac{\sin^2 t}{D^3} + \frac{3}{4D} \right] \epsilon_1^2 + \end{aligned} \quad (56)$$

(continued)

$$\begin{aligned}
& + \left[\frac{\sin^3 t}{D^4} + \frac{3\sin(t)}{4D^2} \right] \epsilon_1^3 \\
& + \left[\frac{3(-1+2G)\cos\theta}{4D} - \frac{\cos\theta\sin^2 t}{D^3} \right] \epsilon_1^2 \epsilon_2 \quad (56) \\
& - \frac{\sin(t)\cos^2\theta}{2D^2} \epsilon_1 \epsilon_2^2 - \frac{\cos^3\theta}{2D} \epsilon_2^3 \quad (\text{cont.})
\end{aligned}$$

It is interesting that the term in $\epsilon_1^2 \epsilon_2$ is the first one influenced by G .

In evaluating the integral of Eq. (44), it will be assumed that ϵ_1 and ϵ_2 are sufficiently small so that the first three terms of (56) are a good approximation to P . Then the integral becomes

$$\begin{aligned}
\int_0^{\frac{L}{R}} \int_0^\pi P \cos\theta d\theta dZ &= \left[-\frac{\pi L}{2R} - \frac{\pi L^3}{32R^3}(\phi')^2 - \frac{\pi L^5}{256R^5}(\phi')^4 - \dots \right] \epsilon_2 \\
&+ \left[\frac{\pi L}{2R}(1+2\epsilon_1 \sin(t)) + \frac{3L^3\pi}{32R^3}(\phi')^2(1+4\epsilon_1 \sin(t)) + \dots \right] Y \\
&+ \left[-\frac{3\pi L}{8R} - \frac{5\pi L^3}{32R^3}(\phi')^2 + \dots \right] \epsilon_2 Y^2 \\
&+ \left[\frac{3\pi L}{8R}(1+4\epsilon_1 \sin(t)) + \dots \right] Y^3 \\
&+ \left[-\frac{5\pi L}{16R} - \dots \right] \epsilon_2 Y^4 + \dots
\end{aligned} \quad (57)$$

In the derivation of this equation, the denominators of the P terms were expanded in series, and only the first five terms of these series were considered. The dots (\dots) inside the square brackets of the terms of Eq. (57) indicate that there would be additional terms if more terms of these denominator terms had been used. The dots

at the end of (57) indicate that there would be additional terms there if more terms of (56) had been used.

Equation (57) is written in ascending powers of Y because it is the integral for the equation of motion in the Y coordinate. Motion in ϕ' can affect motion in Y only through this integral, and it should be clear that such effects are present only for terms in even powers of ϕ' .

If the integral of Eq. (48) is evaluated in a similar manner to that above, the result is

$$\begin{aligned} \int_0^{\frac{L}{R}} \int_0^\pi P(Z - \frac{L}{2R}) \cos \theta d\theta dZ &= \frac{\pi L^3}{24R^3} \left[(1 + 2\epsilon_1 \sin(t)) - \frac{3\epsilon_2}{2} Y \right. \\ &\quad \left. + \frac{9}{4}(1 + 4\epsilon_1 \sin(t)) Y^2 - \frac{5\epsilon_2}{2} Y^3 + \dots \right] \phi' \\ &\quad + \frac{3\pi L^5}{640R^5} \left[(1 + 4\epsilon_1 \sin(t)) - \frac{10\epsilon_2}{3} Y + \dots \right] (\phi')^3 + \dots \end{aligned} \quad (58)$$

It should be clear from this equation that all powers of Y affect motion in the ϕ' coordinate.

Now that the nature of the coupling between the coordinates has been discussed, assume that Y and ϕ' are so small that Eqs. (57) and (58) can be approximated as

$$\int_0^{\frac{L}{R}} \int_0^\pi P \cos \theta d\theta dZ \simeq -\frac{\pi L \epsilon_2}{2R} + \frac{Y \pi L}{2R} (1 + 2\epsilon_1 \sin(t)) \quad (59)$$

and

$$\int_0^{\frac{L}{R}} \int_0^\pi P(Z - \frac{L}{2R}) \cos \theta d\theta dZ \simeq \frac{\pi L^3}{24R^3} (1 + 2\epsilon_1 \sin(t)) \phi' \quad (60)$$

Substituting (59) into (44) gives

$$\frac{d^2 Y}{dt^2} + \frac{\pi}{B}(1+2\epsilon_1 \sin(t))Y = \frac{\pi \epsilon_2}{B} - \frac{2W'}{B} \quad (61)$$

If $Y+\Delta Y$ is substituted for Y in this equation, where both Y and $Y+\Delta Y$ are solutions of the equation, for slightly different sets of initial conditions, the following variational equation in ΔY results:

$$\frac{d^2(\Delta Y)}{dt^2} + \frac{\pi}{B}(1+2\epsilon_1 \sin(t))(\Delta Y) = 0 \quad (62)$$

This is a form of the Mathieu equation, about which more will be said later.

If Eq. (60) is substituted into (48), the equation in ϕ' becomes:

$$\frac{d^2 \phi'}{dt^2} + \frac{\pi L^2}{BR^2 \left[3 + \left(\frac{L}{R} \right)^2 \right]} (1+2\epsilon_1 \sin(t)) \phi' = 0 \quad (63)$$

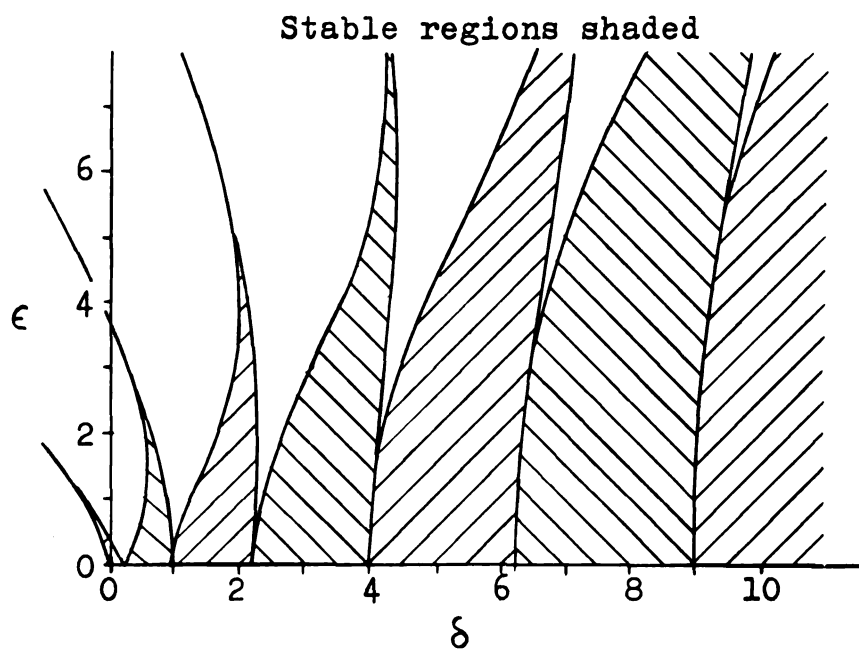
This is already a form of the Mathieu equation; thus, there is no need to use the variational method.

The Mathieu equation is one for which the regions of stability are well-known. For a Mathieu equation in the form

$$\frac{d^2 w}{dq^2} + (\delta + \epsilon \sin(q))w = 0, \quad (64)$$

the regions of stability in the ϵ - δ plane are indicated in Fig. 25 (This figure was taken from Ref. [18]). Note that the stable regions of this plot are connected together at points where $\epsilon = 0$, $\delta = \frac{n^2}{4}$, n an integer.

Fig. 25.--Stable and unstable regions
for the Mathieu equation.



Because Eqs. (62) and (63) are both Mathieu equations, it should be clear that a plot of $\frac{2\epsilon_1\pi}{B}$ versus $\frac{\pi}{B}$ for the Y coordinate would be similar to Fig. 24, as would a plot of $\frac{2\epsilon_1\pi L^2}{BR^2\left[3+\left(\frac{L}{R}\right)^2\right]}$ versus $\frac{\pi L^2}{BR^2\left[3+\left(\frac{L}{R}\right)^2\right]}$ for the Φ' coordinate. In this work, however, these are not the quantities which have been plotted, although plots of ϵ_1 versus $\frac{1}{B}$, such as have been used in the one-degree-of-freedom case, lend themselves to an observation based on the Mathieu plot.

Consider $\frac{2\epsilon_1\pi}{B}$ to be plotted against $\frac{\pi}{B}$ for the stability regions of the Y coordinate, thus giving a Mathieu plot, at least for small ϵ_1 and ϵ_2 . The first and second stable regions of such a plot should come together at $\frac{2\epsilon_1\pi}{B} = 0$, $\frac{\pi}{B} = \frac{1}{4}$, as indicated previously for Mathieu plots. On a plot of ϵ_1 versus $\frac{1}{B}$, this same point would occur at $\epsilon_1 = 0$, $\frac{1}{B} = \frac{1}{4\pi} = 0.0796$. Refer to Fig. 16 again, and consider the curve for $W' = 0.001$. With this low value of W' at the lowest point of the curve (low ϵ_1), ϵ_2 should also be small, so the present approximate analysis should apply. At the lowest point of this curve, the value of $\frac{1}{B}$ is 0.067, which does not agree exactly with the value predicted above, but is definitely of the same order of magnitude. If the downhill portion of this curve is extended to the abscissa as shown, the intersection occurs at $\frac{1}{B} = 0.078$. This is much closer to the predicted value, as should be expected since this point

corresponds to $\epsilon_1 = \epsilon_2 = W' = 0$, all parameters as small as possible. This analysis indicates that only the first stable region of the Mathieu plot is of interest in the present gas-bearing work.

If an argument similar to the one above is applied to the equation for the ϕ' coordinate, it would be found that the intersection of the first two stability boundaries with the abscissa would occur at $\frac{\pi L^2}{BR^2 \left[3 + \left(\frac{L}{R} \right)^2 \right]} = \frac{1}{4}$, or at $B^{-1} = 0.0796 \left[1 + 3 \left(\frac{R}{L} \right)^2 \right]$. It should be clear that for an infinitely-long bearing, this expression reduces to the value given above for the Y coordinate; also, as $\frac{L}{R}$ approaches zero, the value of this expression approaches infinity. Thus, if the stability boundaries for both the Y and ϕ' coordinates are plotted on the same ϵ_1 -versus- B^{-1} plot, the stability region for ϕ' should be at least as large as the region for Y, regardless of the value of $\frac{L}{R}$. This conclusion should be valid at least in the small-parameter regions, and, if the value of B^{-1} at the abscissa for the Y coordinate is known, it should be possible to calculate the corresponding B^{-1} for ϕ' by using

$$(B^{-1})_{\phi'} = \left[1 + 3 \left(\frac{R}{L} \right)^2 \right] (B^{-1})_Y \quad (65)$$

While this development was based on small-parameter considerations, it will be seen in the next section that Eq. (65) proved to be quite accurate over a large part of the stability map.

The analysis of the present section led to two main observations, which are restated here for future reference: 1) Unless ϕ' or $\frac{d\phi'}{dt}$ is given some initial value other than zero, no subsequent motion in ϕ' will occur, and 2) For small ϵ_1 , ϵ_2 , Y , and ϕ' , the stability regions in the ϕ' coordinate are always at least as large as those in the Y coordinate.

While Eq. (65) was stated above for an ϵ_1 -versus- B^{-1} plot near the abscissa, it should be valid for any plot using B^{-1} as the abscissa variable, provided ϵ_1 and ϵ_2 are still small. In particular, it should hold for plots of ϵ_2 versus B^{-1} at constant ϵ_1 , such as were used earlier in the single-degree-of-freedom cases, at least for curves of low ϵ_1 where they approach the abscissa. This is pointed out here because the computer work discussed in the next section was all carried out in the ϵ_2 -versus- B^{-1} plane.

Some Computer Results for Two Degrees of Freedom

Because of the long computer times required, it was found impractical for present purposes to determine complete sets of stability curves in two degrees of freedom. Instead, only a few single points on the stability boundary were located for various combinations of parameters, and the results so obtained are discussed in terms of the observations made above.

In the single-degree-of-freedom work, the initial

value of Y was defined in terms of a parameter CRD , which was the decimal fraction of the minimum Y for instability. In this two-degree-of-freedom work, CRD is retained, but is now the decimal fraction of the minimum Y for instability with ϕ' equal to zero. In order to provide for different-sized starting angles, a parameter $CRD2$ is similarly defined as the decimal fraction of the minimum ϕ' for instability with Y equal to zero. Both CRD and $CRD2$ can be given values between zero and unity, but if their sum equals or exceeds unity, the bearing will be unstable at the start.

Since the first observation of the preceding section was based on the equation in ϕ' with no limiting assumptions, it is felt to be unquestionably valid, and any comparison between it and computer runs starting with $\phi' = \frac{d\phi'}{dt} = 0$ would serve more to check the computer program than the observation. In any computer runs which were made with these starting conditions, ϕ' remained equal to zero as predicted by the observation, except in regions of instability, and in these cases it was concluded that cumulative errors in the computer were the cause of eventual motion in ϕ' .

Computer verification of the second observation was even better than expected. Since this observation--that stability regions in ϕ' would be at least as large as those in Y --was based on a small-parameter analysis, it

was anticipated that it might apply only in limited regions. However, as will be seen below, it proved to be applicable for much of the stability plot.

The first method used to determine the effects of the second degree of freedom on stability was to simply make computer runs with motion in both coordinates permitted. Because too much computer time would have been required to establish complete curves of the type shown in Fig. 21, only single boundary points were found for a number of cases. For most of these cases, the point arbitrarily chosen for test was $\epsilon_1 = 0.3$, $\epsilon_2 = -0.1$, $\frac{L}{R} = 2$. A number of runs was made at this point, starting with various combinations of CRD and CRD2, and, although the boundary point determined sometimes varied slightly, motion in ϕ' was never the reason for instability. In one particular sequence, CRD was held at zero while CRD2 was increased in steps of 0.1 from zero to 0.6. In all of these runs, ϕ' was well-behaved. Its general tendency was to oscillate with approximately its initial amplitude, while only Y exhibited any oscillations of growing amplitude. At the time these runs were made, it had not yet been predicted that longer bearings would be less stable in the angular coordinate. Possibly choosing an $\frac{L}{R}$ of 2 made these results more clear-cut than they might have been for a larger value, but a similar case to be discussed later, with $\frac{L}{R} = 10$, yields the same general conclusion.

Motion in the Angular Coordinate Only

Although it seemed clear at this point that motion in the Y coordinate would be the dominating cause of any instability, it was still desired to verify that unstable regions do exist for motion in the ϕ' coordinate. In order to do this, it was necessary to modify the computer program so that instability in Y could not occur. This was done by holding Y at its equilibrium value, $Y = \epsilon_2$, thus allowing only tilting of the journal about its center of gravity. Again because of limited computer time, only single points were located in most of these runs. For a given combination of values of ϵ_1 , ϵ_2 , and $\frac{L}{R}$, the corresponding value of B^{-1} was predicted using Eq. (65) and the plots of Fig. 21. Then the values of ϵ_1 , ϵ_2 , and $\frac{L}{R}$ were read into the computer, and the start-up procedure of the original program was used to locate just the first point on the stability boundary. For all of these cases, the value of CRD2 was 0.1.

Table 1 summarizes the results of these runs. The first point tested was at $\epsilon_1 = 0.3$, $\epsilon_2 = -0.1$ for various values of $\frac{L}{R}$. The agreement between predicted and calculated values of B^{-1} at this point was excellent. Thus, subsequent tests were made along the curve of constant ϵ_1 ($=0.3$) for various ϵ_2 and $\frac{L}{R}$, and along the line of constant ϵ_2 ($=-0.1$) for various ϵ_1 and $\frac{L}{R}$. Agreement between predicted and calculated values is good for this latter series, possibly because the value of ϵ_2 is small,

Table 1.--Comparison of computed values of B^{-1}
with those predicted by Eq. (65).

ϵ_1	ϵ_2	$\frac{L}{R}$	CRD	CRD2	Pred. B^{-1}	Comp. B^{-1}
0.3	-0.100	2.0	0.0	0.1	0.0788	0.079
0.3	-0.100	5.0	0.0	0.1	0.0504	0.050
0.3	-0.100	10.0	0.0	0.1	0.0463	0.046
0.3	-0.100	100.0	0.0	0.1	0.0450	0.045
0.3	-0.300	1.0	0.0	0.1	0.1507	0.149
0.3	-0.300	2.0	0.0	0.1	0.066	0.065
0.3	-0.300	10.0	0.0	0.1	0.0388	0.039
0.3	-0.500	1.0	0.0	0.1	0.0952	0.087
0.3	-0.500	2.0	0.0	0.1	0.0416	0.038
0.3	-0.500	10.0	0.0	0.1	0.0245	0.023
0.4	-0.100	1.0	0.0	0.1	0.138	0.138
0.4	-0.100	2.0	0.0	0.1	0.0604	0.060
0.4	-0.100	10.0	0.0	0.1	0.0355	0.035
0.5	-0.100	1.0	0.0	0.1	0.0988	0.100
0.5	-0.100	2.0	0.0	0.1	0.0432	0.044
0.5	-0.100	10.0	0.0	0.1	0.0254	0.026
0.6	-0.100	1.0	0.0	0.1	0.0648	0.066
0.6	-0.100	2.0	0.0	0.1	0.0284	0.029
0.6	-0.100	10.0	0.0	0.1	0.0167	0.017
0.4	-0.435	1.0	0.0	0.1	0.0692	0.060
0.5	-0.325	1.0	0.0	0.1	0.0576	0.053
0.6	-0.245	1.0	0.0	0.1	0.0420	0.039
0.4	-0.435	2.0	0.0	0.1	0.0303	0.027
0.5	-0.325	2.0	0.0	0.1	0.0252	0.023
0.6	-0.245	2.0	0.0	0.1	0.0184	0.0169
0.6	-0.245	10.0	0.0	0.1	0.0108	0.0105

but for the point at $\epsilon_1 = 0.3$, $\epsilon_2 = -0.5$, the difference between the two values of B^{-1} is significant.

The last points tested were located just before the entrances to the holes of Fig. 21 for $\epsilon_1 = 0.4, 0.5, 0.6$. These results are also given in Table 1, and, although there is again a noticeable difference between the two values of B^{-1} , the largest difference in any case is only 0.0092. Fortunately, the largest discrepancies in Table 1 occur for smaller values of $\frac{L}{R}$, and, since the ϕ' -stability region for such cases is considerably larger than the accompanying Y -stability region, such discrepancies can be safely ignored. Note that the largest difference between predicted and computed values of B^{-1} for $\frac{L}{R}$ of 10 is only 0.0015.

Several attempts were made to locate holes in the ϕ' -stability region. The first approach was to start the automatic program just below the suspected hole entrance for $\epsilon_1 = 0.3$, $\frac{L}{R} = 10$, and to let the program find the hole. Two ten-minute runs on the computer located only nine boundary points. Since the suspected entrance had been passed with no tendency of the program to turn in to it, it was decided to try another method. Single points were tested along a line of constant ϵ_2 ($= -0.55$), starting from the already-established right-hand boundary and moving left in an attempt to locate other unstable points; none were found. Similar testing was done in the anticipated hole regions for other values of ϵ_1 , and

again no holes were found. Apparently either there are no hole regions in the ϕ' stability plots, or else more cycles should be required as the criterion for stability in these regions. Because the ϕ' response plots obtained for fifty cycles of test showed no tendency toward going unstable in the near future, it was decided not to run the cases for a larger number of cycles, but to continue on the assumption that these points would remain stable in ϕ' indefinitely.

Back to Motion in Both Coordinates

The main reason for testing for stability in ϕ' alone was to verify that stable and unstable regions do exist for this coordinate. It was anticipated that the boundaries of these regions might be difficult to locate without constraining the motion in Y, since instability might always occur in Y first. The above results verify that the region of stability for ϕ' alone is always at least as large as the corresponding region for Y alone. This suggests that it might be possible to predict stability characteristics in both coordinates on the basis of the stability plots for Y alone.

As mentioned earlier, the point at $\epsilon_1 = 0.3$, $\epsilon_2 = -0.1$, $\frac{L}{R} = 2$, was tested with motion being allowed in both coordinates. The boundary point located was identical to the one given in Fig. 21 for motion in Y only. This agreement is not surprising, since, for $\frac{L}{R} = 2$, the sta-

bility region in ϕ' is expected to be 1.75 times as large as that in Y ; thus, motion in ϕ' should have very little influence on the stability of the bearing as a whole. If motion in the angular coordinate is ever apt to reduce the size of the stability region for the bearing as a whole, it seems that it would be most likely to do so for larger values of $\frac{L}{R}$.

It was mentioned before that the automatic program was allowed to locate nine points near the entrance to the hole for $\epsilon_1 = 0.3$, $\frac{L}{R} = 10$, with motion being allowed only in ϕ' . Until the suspected hole region was reached, the resulting stability plot for ϕ' was practically on top of the one given for Y in Fig. 21. Since the plots for each of the separate coordinates were known in this region, it was decided that this is where stability in both coordinates simultaneously should be tested. Starting from the same point as for the ϕ' -only run, with $\frac{L}{R} = 10$, $CRD = 0.$, $CRD2 = 0.1$, the automatic program was allowed to run for ten minutes, locating four good points. The section of boundary defined by these points was only slightly to the left of that given in Fig. 21.

It was not surprising that the stability region was reduced for the two-degree-of-freedom system, since amplitudes of Y and ϕ' which would survive the stability test alone now had to pass it together. However, the response plots in ϕ' for the stable points of this run

seemed to be growing in amplitude near the point of cut-off at fifty cycles. A retest of these same points for 250 cycles of squeeze revealed that the motion in ϕ' was of a beating nature, and the increasing amplitude observed after fifty cycles was just the peak of the first beat.

CONCLUSIONS

The stability characteristics of journal bearings under various constraints have been investigated.

Starting with the results of Ref. [11], the automatic technique was applied to locate holes in the stability regions for infinite journals. Extensions of the analysis to (1) bearings of finite length and (2) bearings allowed to tilt as well as translate in one plane led to larger stable regions than those given for the infinite journal. Because the equations of motion for the remaining two coordinates are essentially of the same form as those already tested, especially for small parameters, it is felt that an extension of the computer analysis to more coordinates would lead to very little new information, and such information would come only at the expense of a great amount of computer time.

If further work is to be done, other extensions than increasing the number of coordinates would probably be more worthwhile. For examples, the squeeze-film bearing might be analyzed with the journal rotating, periodic loads might be considered, or an applied torque might be added to the ϕ' coordinate. There is obviously much more work which could be done in this area, but un-

til such time as individual cases can be considered in detail, it seems advisable to keep points of operation of any journals within the stability regions of infinite journals. Bearing designs based on this requirement would at least be conservative when operated under the conditions specified in this paper.

LIST OF REFERENCES

1. J. V. Beck and C. L. Strodtman, "Stability of a Squeeze-Film Journal Bearing", ASME Paper No. 66-Lub-15, presented at the ASME-ASLE Lubrication Conference, Minneapolis, Minn., October 18-20, 1966.
2. W. A. Gross and E. C. Zachmanoglou, "Perturbation Solutions for Gas-Lubricating Films", Journal of Basic Engineering, ASME Transactions, vol. 83, pp. 139-144, June, 1961.
3. J. S. Ausman, "An Improved Analytical Solution for Self-Acting, Gas-Lubricated Journal Bearings of Finite Length", Journal of Basic Engineering, ASME Transactions, vol. 83, pp. 188-194, June, 1961.
4. H. S. Cheng and P. R. Trumpler, "Stability of the High-Speed Journal Bearing Under Steady Load, Part 2--The Compressible Film", Journal of Engineering for Industry, ASME Transactions, vol. 85, pp. 274-280, August, 1963.
5. H. S. Cheng and C. H. T. Pan, "Stability Analysis of Gas-Lubricated, Self-Acting, Plain, Cylindrical Journal Bearings of Finite Length, Using Galerkin's Method", Journal of Basic Engineering, ASME Transactions, vol. 87, pp. 185-192, March, 1965.
6. V. Castelli and H. G. Elrod, Jr., "Solution of the Stability Problem for 360 Degree Self-Acting, Gas-Lubricated Bearings", Journal of Basic Engineering, ASME Transactions, vol. 87, pp. 199-212, March, 1965.
7. J. S. Ausman, "Linearized Stability Theory for Translatory Half-Speed Whirl of Long, Self-Acting Gas-Lubricated Journal Bearings", Journal of Basic Engineering, ASME Transactions, vol. 85, pp. 611-619, December, 1963.

8. Y. Katto and N. Soda, "Theoretical Contributions to the Study of Gas-Lubricated Journal Bearings", Journal of Basic Engineering, ASME Transactions, vol. 84, pp. 123-131, March, 1962.
9. C. H. T. Pan and B. Sternlicht, "Comparison Between Theories and Experiments for the Threshold of Instability of Rigid Rotor in Self-Acting, Plain-Cylindrical Journal Bearings", Journal of Basic Engineering, ASME Transactions, vol. 86, pp. 321-327, June, 1964.
10. E. O. J. Salbu, "Compressible Squeeze Films and Squeeze Bearings", Journal of Basic Engineering, ASME Transactions, vol. 86, pp. 355-366, June, 1964.
11. C. H. T. Pan, S. B. Malanoski, P. H. Broussard, Jr., and J. L. Burch, "Theory and Experiments of Squeeze-Film Gas Bearings, Part 1--Cylindrical Journal Bearing", Journal of Basic Engineering, ASME Transactions, vol. 88, pp. 191-198, March, 1966.
12. W. A. Gross, Gas Film Lubrication, John Wiley and Sons, Inc., New York, 1962.
13. J. V. Beck and C. L. Strodman, "Squeeze-Film Bearing: Infinitely-Long Flat Plate", Lear-Siegler Incorporated, Engineering Memo Report Number 186, September 17, 1965.
14. H. G. Elrod, Jr., Notes of meeting at Lear-Siegler Incorporated, Grand Rapids, Michigan, December 28-30, 1964.
15. S. H. Crandall, Engineering Analysis, McGraw-Hill Book Co., Inc., New York, 1956.
16. J. V. Beck and C. L. Strodman, "Mass-Content Rules for Squeeze-Film Gas Bearings", Lear-Siegler Incorporated, Engineering Memo Report Number 192, June 17, 1966.
17. D. W. Peaceman and H. H. Rachford, Jr., "The Numerical Solution of Parabolic and Elliptical Differential Equations", Journal of the Society for Industrial and Applied Mathematics, vol. 3, pp. 28-41, 1955.
18. J. J. Stoker, Nonlinear Vibrations in Mechanical and Electrical Systems, Interscience Publishers, Inc., New York, 1950.

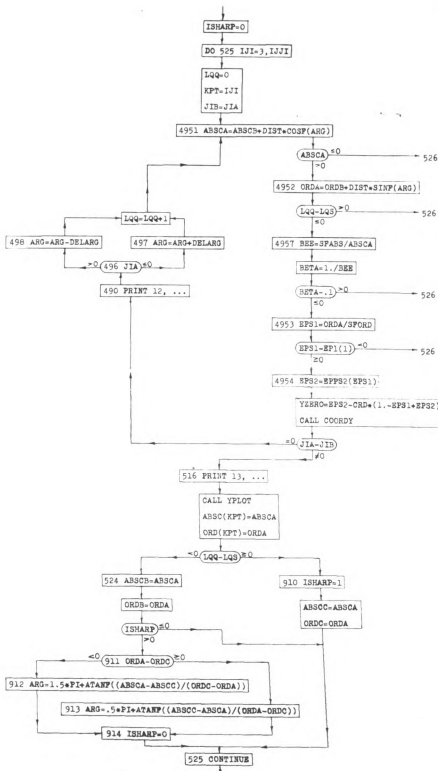
APPENDIX A

This appendix presents the portion of one of the computer programs which includes the logic for automatic curve following. Specifically, the program from which the following statements are taken is the one which was used to follow the curve for $W'=0.001$ in Fig. 16; thus the sharp-turn logic in this listing is the best one which was developed. Fig. A-1 is a flow chart of the portion of program being discussed. Following is the **FORTRAN** listing of the same portion of program including numerous descriptive comments. It is felt that the best way to gain an understanding of how this method works is to apply it by hand to a section of sketched curve, preferably one with a sharp turn in it. It should be noted that, in this particular program, the stable region is on the right-hand side of the boundary as the program progresses. This was not the case in all programs used, but only minor modifications are necessary to develop one from another.

The FORTRAN Listing

Previous to this point in the program, two starting points A and B are located by the method used in Ref. [1], and their ordinate and abscissa values are

Fig. A-1.--Flow chart for the automatic curve-following logic.



named ABSCA, ORDA, ABSCB, and ORDB. The values of these quantities are changed throughout the following DO-loop, with each new B being the previous A and each new A being calculated from statements 4951 and 4952 below.

ISHARP=0

This is the value which ISHARP will have unless a 180° change of direction is made in searching for the next point. Discussed further below.

DO 525 IJI=3,IJJI

IJJI is read into the program earlier as the total number of points that it is desired to test.

LQQ=0

LQQ is set equal to zero at the beginning of each run through the DO-loop, and it is increased by 1 each time ARG is changed. If ARG is changed enough times in searching for a new point, LQQ will equal LQS (defined earlier in the program), indicating a sharp turn. When this occurs, the sharp-turn logic is applied below.

KPT=IJI

JIB=JIA

SUBROUTINE COORDS, which tests for stability at each point, assigns a value of 0 to JIA for stable points and 1 for unstable points. At this point in the program, JIB is given the value of JIA for the last point tested. Subsequent points are tested until the value of JIA returned by COORDS no longer equals JIB; this indicates that the boundary has been crossed. Then the DO-loop is completed for that value of IJI, and the process is repeated.

GO TO 4951

490 PRINT 12, ...

Format statement 12 is used to print information concerning points tested but not kept.

496 IF(JIA) 497,497,498

If JIA is zero, statement 497 will cause ARG to be increased by DELARG, indicating a left turn toward the unstable region. If JIA is 1, statement 498 will decrease ARG by DELARG, indicating a right turn toward the stable region.

497 ARG=ARG+DELARG

LQQ=LQQ+1

GO TO 4951

498 ARG=ARG-DELARG

LQQ=LQQ+1

4951 ABSCA=ABSCB+DIST*COSF(ARG)

This gives the abscissa value of the next point to be tested.

IF(ABSCA) 526,526,4952

If the abscissa value of the next point is less than or equal to zero, the program goes to statement 526 (not included here) and terminates the run for that set of data; otherwise, it continues to statement 4952.

4952 ORDA=ORDB+DIST*SINF(ARG)

This gives the ordinate value for the next point.

IF(LQQ-LQS) 4957,4957,526

For certain values of DELARG which might be read in to the program, it is possible that the incrementing of ARG might continue indefinitely without crossing the

stability boundary. This statement limits the turn to about 180° before the case is terminated at statement 526. This is not likely to be a problem if DELARG is divisible into 180° a whole number of times.

4957 BEE=SFABS/ABSCA

BEE is the B of the main text. SFABS and SFORD (below) were scale factors provided for the abscissa and ordinate in case it was found convenient to expand one of the scales for the search. Values for these quantities were read in to the program as data, but the flexibility thus provided was not used.

BETA=1./BEE

IF(BETA-.1) 4953,4953,526

This statement prevents the search from going indefinitely to the right; it is what terminated the curve of Fig. 16 for $W'=0.001$.

4953 EPS1=ORDA/SFORD

IF(EPS1-EP1(1)) 526,4954,4954

This program was one of the ones which interpolated in a table of EPS1 and EPS2 to get the value of EPS2 at each new point. The array of EPS1 values was EP1. This statement causes the program to terminate if the value of EPS1 at hand is lower than the lowest value in the EP1 array.

4954 EPS2=EPPS2(EPS1)

EPPS2 was the function subroutine which did the interpolation mentioned above.

YZERO=EPS2-CRD*(1.-EPS1+EPS2)

This sets the initial value of Y as prescribed by Eq. (28).

CALL COORDY

COORDY was the subroutine which tested for stability and returned the correspond-

ing values of JIA.

IF(JIA-JIB) 516,490,516

See the above comment under the statement JIB=JIA.

516 PRINT 13, ...

Format statement 13 was used to print out data which proved to be on the boundary.

CALL YPLOT

YPLOT was the subroutine used to plot the responses of the type given in Figs. 8, 9, and 10.

ABSC(KPT)=ABSCA

ORD(KPT)=ORDA

ABSC and ORD were arrays for storage of the values used to plot the curves such as Fig. 16 after all points on the curve were tested for stability.

IF(LQQ-LQS) 524,910,910

This is the test to determine whether the sharp-turn logic should be used. It should be used if LQQ is greater than or equal to LQS.

910 ISHARP=1

ABSCC=ABSCA

ORDC=ORDA

These last three values are used in the sharp-turn logic on the next trip through the loop.

GO TO 525

524 ABSCB=ABSCA

ORDB=ORDA

Point A becomes the new point B, and memory locations for ABSCA and ORDA are

available for new values the next time through statements 4951 and 4952.

IF(ISHARP) 525,525,911

If ISHARP had been set equal to 1 on the previous trip through the loop, the program would go to statement 911 to continue the sharp-turn logic; otherwise it would go on to statement 525.

911 IF(ORDA-ORDC) 912,913,913

The sharp-turn logic defines a new starting ARG based on either statement 912 or 913. Which one is used depends on the value of (ORDA-ORDC).

912 ARG=1.5*PI+ATANF((ABSCA-ABSCC)/(ORDC-ORDA))

GO TO 914

913 ARG=.5*PI+ATANF((ABSCC-ABSCA)/(ORDA-ORDC))

914 ISHARP=0

ISHARP is reset at zero here so that the sharp-turn logic will be bypassed until the next time a sharp turn is encountered.

525 CONTINUE

MICHIGAN STATE UNIVERSITY LIBRARIES



3 1293 03169 0211